AUTONOMOUS VEHICLES

Advancing physical intelligence for autonomous soft robots

Chi Chen[1], Pengju Shi[1], Zixiao Liu[1], Sidi Duan[1], Muqing Si[1], Chuanwei Zhang[1], Yingjie Du[1], Yichen Yan[1], Timothy J. White[2,3], Rebecca Kramer-Bottiglio[4], Metin Sitti[5], Tetsuya Iwasaki[6], Ximin He[1]*

Achieving lifelike autonomy remains a long-term aspiration, yet soft robots so far have mostly demonstrated rudimentary physical intelligence that relies on manipulation of external stimuli to generate continuous motion. To realize autonomous physical intelligence (API) capable of self-regulated sensing, decision-making, and actuation, a promising approach is creating nonlinear time-lag feedback embedded within materials, where a constant stimulus elicits delayed responses to enable autonomous motion. This Review explores such feedback mechanisms, traces the evolution of physically intelligent robots, outlines strategies for embedding API in soft robots under diverse environments, and further discusses challenges and future directions beyond simple locomotion.

INTRODUCTION

In nature, living organisms respond to external stimuli differently on the basis of their biological intelligence. Whereas many highly evolved creatures communicate with external stimuli through a nerve network, other living organisms such as fungi, microorganisms, and cephalopods operate without using a centralized nervous system or conscious thought—their responses are directly encoded into their bodies. To reproduce such autonomous sensing, decision-making, and actuation in artificial robots, two routes have emerged (Fig. 1). The first is computational intelligence (*1*–*3*), which focuses on the integration of modules controlled by algorithms in a centralized processor or distributed processors. As chip technology and algorithms have evolved, conventional robots have been able to achieve more complex motions with faster response rates. However, there is still exponential difficulty in organically integrating multiple functions, especially in the case of miniaturized, lightweight robots (*4*).

The second alternative solution is to directly embed physical intelligence (decentralized intelligence) in the materials/body, mimicking single-cell behavior in sensing and actuating without a network of nerves (*5*). In contrast with conventional robots, the emergence of soft robots potentially solves the above problems at the material level featuring low cost, ease of fabrication, and inherent mechanical compliance (*6*). More importantly, soft robots based on stimulus-responsive materials can interact with external stimuli, simultaneously performing wide-range sensing and high–degree-of-freedom actuation (*7*), even under untethered natural energy sources (e.g., heat, light, humidity, and chemical), because every part of the material can function as both a sensor and an actuator (*8*, *9*). Nevertheless, most robotic motion continues to rely on human intervention of the stimulus source (e.g., turning on/off or programming the stimulus source) (*10*, *11*), which is far from the autonomous mechanical responses observed in natural systems. Achieving such autonomy requires the ability to control the robot without artificial modulation of the external stimulus fields (*12*). Such a higher level of physical intelligence is herein termed autonomous physical intelligence (API), which can be regarded as a step toward constructing responsive artificial organism systems composed of soft materials. Thus, the question of how such intelligent behavior can be built on inanimate and unconscious components is posed.

Nature has left clues—different feedback mechanisms that drive the self-sensing, self-deciding, and self-regulating evolution of natural systems. Natural systems are often out of equilibrium when subjected to external forces and mass transport (*13*). This disturbance of equilibrium has distinct fates: amplification, pushing the system further away from the initial state and leading to intensified deviation; or stabilization, reducing or eliminating the deviation to bring the system back to an equilibrium state (*14*). The former response to disturbance is termed positive feedback, exemplified by the ice-albedo feedback in the Earth climate system—an initial rise in temperature causing ice and glaciers to melt, exposing land and water beneath with a lower albedo (reflectivity) than ice. This facilitates the absorption of sunlight, further increasing temperature (*15*). On the other hand, if the system response mitigates the initial disturbance, negative feedback is formed. In many cases, the deviation vanishes, and the system retains its equilibrium, exemplified by the fluctuation in blood glucose concentration regulated by synchronized changes in insulin and glucagon, maintaining a dynamic balance of the blood glucose level (*16*)—physiologist Walter N. Cannon coined the word "homeostasis" to describe such a stabilizing effect via negative feedback to regain equilibrium in physiological systems (*17*). In engineering, such negative feedback is used to minimize mechanical instability, e.g., in the case of proportional-integral-derivative control (*18*).

Interestingly, in some special cases, the fluctuation around the equilibrium state can be perpetuated. A famous experiment of the pupil-light reflex demonstrates the steady oscillation of pupil size when a narrow light beam irradiates the edge of the pupil (*19*). Upon irradiation, the pupil contracts to reduce incoming light. Because the pupil response has an ~300-ms delay to light influx, it continues to contract after light is no longer admitted into the retina, until the eye realizes there is no light and enlarges again. The lagged

[1]Department of Material Science and Engineering, University of California, Los Angeles, Los Angeles, CA, USA. [2]Department of Chemical and Biological Engineering, University of Colorado, Boulder, Boulder, CO, USA. [3]Materials Science & Engineering Program, University of Colorado, Boulder, Boulder, CO, USA. [4]School of Engineering & Applied Science, Yale University, New Haven, CT, USA. [5]School of Medicine and College of Engineering, Koç University, Istanbul, Turkey. [6]Department of Mechanical and Aerospace Engineering, University of California, Los Angeles, Los Angeles, CA, USA.
*Corresponding author. Email: ximinhe@ucla.edu

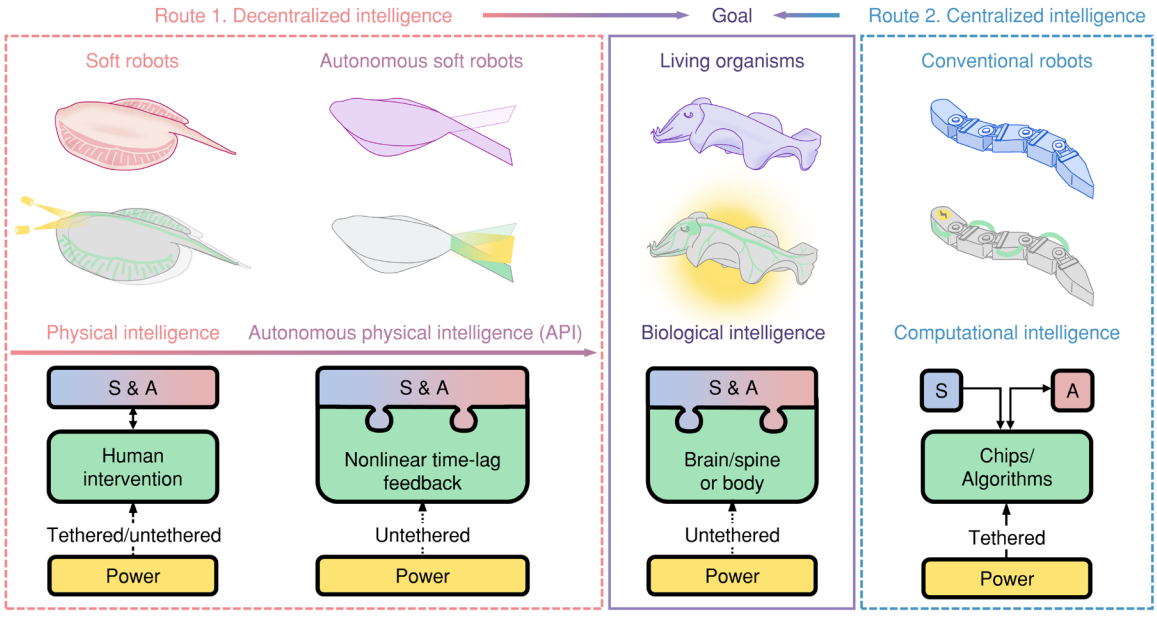

Fig. 1. Two distinct routes for the development of bioinspired robots. The sensing-decision-actuation cycle in robotic systems can be encoded in either the decentralized body (presenting physical intelligence) or a centralized control unit (through computational intelligence), which serve as two parallel routes toward approaching biological intelligence in robots. The sensor (S, blue), actuator (A, red), decision-making component (green), and power supply (yellow) are integrated into the robotic systems in different ways. In particular, API advances physical intelligence by using nonlinear time-lag feedback to perpetuate robotic motion.

response causes pupil expansion to continue after the readmission of the light influx and thus sustains the oscillation of the pupil. In the above case of nonlinear time-lag feedback, the system oscillates steadily because of its intrinsic coupling dynamics, which is generally considered undesirable in engineering given that it may lead to unanticipated and irreversible trends. However, it also offers inspiration to construct systems that continuously interact with the surrounding environment without human intervention and demonstrate lifelike intelligence, a long aspiration in robotic research. To date, a plethora of theoretical and experimental works have used such nonlinear time-lag feedback to achieve self-continuous motion for soft robots performing lifelike locomotion (*11*, *20*, *21*).

In this Review, we first outline the fundamental science of feedback mechanisms, including definitions, key factors, and modeling methodology. Second, we review the evolution of physical intelligence–enabled robots with an increasing level of autonomy under different forms of stimuli. Third, we investigate state-of-the-art strategies of engineering API in soft materials. Last, we explore the demonstration of diverse locomotion modes for autonomous self-continuous soft robots in different environments. We consider that this built-in control mechanism is an essential step in autonomous robotic development toward biological intelligent systems in varying environments.

NONLINEAR TIME-LAG FEEDBACK FOR API

Feedback mechanisms

A dynamic feedback system is a system whose behavior evolves over time, usually in response to external stimulation (*22*). The term feedback refers to a situation where dynamic systems are interconnected in a cycle such that each system influences the other and their dynamics are thus strongly coupled. In many natural and engineered systems, feedback confers on systems the property of being insensitive both to external disturbances and to variations in their internal elements. A simple pendulum can serve as a principal model to illustrate the coupling dynamics and feedback mechanisms between system components, such as the stimulus (input)–response (output) coupling, which is critical for the onset of many autonomous motions. The linearized equation of motion for the pendulum system is a second-order differential equation, given by

$$\begin{aligned} &\text{Pendulum: } \ddot{\theta}+\theta=u \\ &\text{Applied torque: } u=f\left(\dot{\theta}\right) \end{aligned} \tag{1}$$

where $\ddot{\theta}$ is the angular acceleration, θ is the pendulum angle (output), u is the torque applied to the pendulum at the pivot (input), and $f\left(\dot{\theta}\right)$ is a function depending on the angular velocity $\dot{\theta}$ (red solid line in Fig. 2). The mechanical system can be recognized as a feedback system between the applied torque $u=f\left(\dot{\theta}\right)$ and pendulum response θ. The behavior of the pendulum system is completely determined by the initial values of the position θ and the velocity $\dot{\theta}$, and hence $x_1 \coloneqq \dot{\theta}$ and $x_2 \coloneqq \theta$ are called the state variables. By using the state variables, the system can be described as

$$\begin{aligned} \dot{x}_1 &= -x_2+f\left(x_1\right) \\ \dot{x}_2 &= x_1 \end{aligned} \tag{2}$$

The isoclines are defined to be the curves on the (x_1, x_2) plane specified by setting the derivatives to zero (*23*). In particular, $x_2 = f(x_1)$ and $x_1 = 0$ are vertical and horizontal isoclines because the state trajectory (x_1, x_2) crosses the curves vertically ($\dot{x}_1 = 0$) and horizontally ($\dot{x}_2 = 0$), respectively. The intersection of the two isoclines gives the equilibrium point.

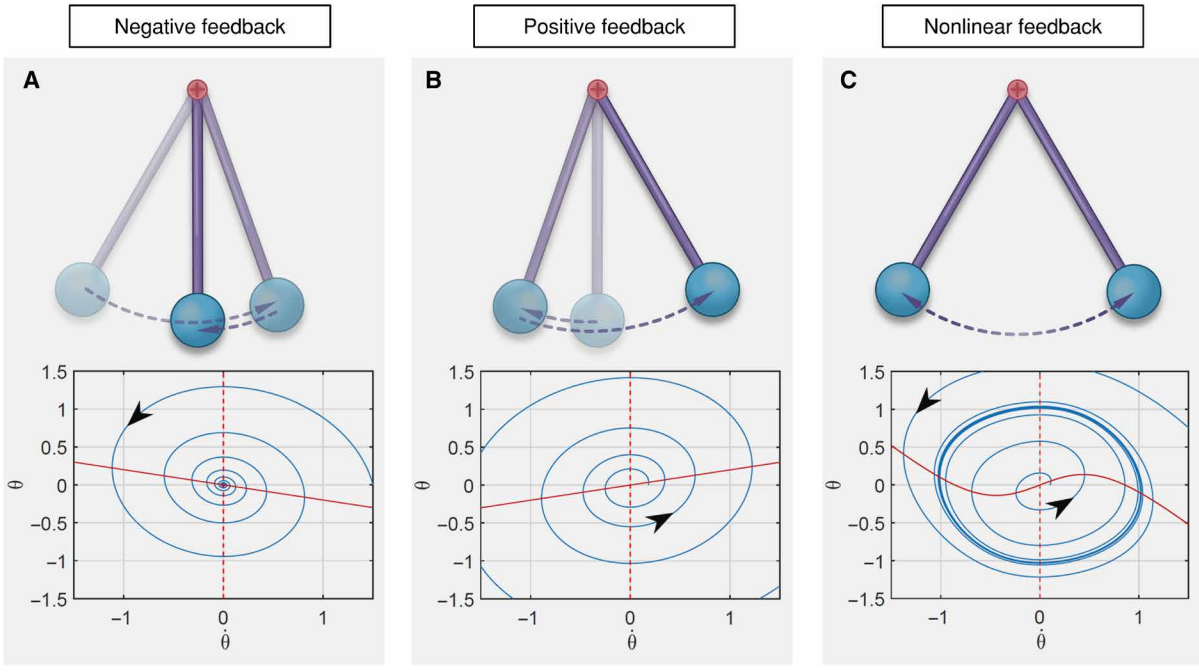

Fig. 2. Comparison of various feedback systems and their trajectories. Different coupling dynamics between two isoclines can lead to (**A**) convergence with negative feedback, (**B**) divergence with positive feedback, and (**C**) oscillation with nonlinear feedback based on both negative and positive effects.

Depending on different conditions (discussed in the next section), the system can decay to an equilibrium state, as in the case that a swinging pendulum eventually becomes static under friction (Fig. 2A), which is an example of negative feedback that stabilizes the equilibrium subject to external disturbance. Specifically, the effect of the viscous friction at the pivot can be modeled by an applied torque $f(\dot{\theta}) = -c\dot{\theta}$ with a positive constant $c > 0$. This results in a negative feedback system because a perturbation in the angular velocity $\dot{\theta}$ results in the applied torque $u = -c\dot{\theta}$ in the opposite direction. The negative feedback makes the angle θ converge (Fig. 2A, bottom), where the state trajectory (blue) on the (x_1, x_2) plane passes through the isoclines (red) horizontally and vertically, spiraling into the stable equilibrium at the origin ($\theta = \dot{\theta} = 0$).

Conversely, positive feedback will drive systems further away from equilibrium by amplifying an existing perturbation due to external disturbances, which generally leads to exponential growth in output. Such behavior is exemplified by a pendulum that is excited each time it reaches a local maximum amplitude, akin to a swing pumped at the right timing (Fig. 2B). Specifically, the negative damping torque acts in the same direction as the angular velocity as in $f(\dot{\theta}) = c\dot{\theta}$, forming a positive feedback loop that magnifies the perturbation. In this case, the equilibrium is unstable, and a small perturbation leads to a divergent oscillation (Fig. 2B). For example, improperly designed self-excited oscillations can evolve into divergent and unstable flutter motions, which are likely to cause structural damage and should be avoided in robotic designs (*24*, *25*). Through an engineered mechanism, it is possible to achieve stable oscillation with nonlinear feedback with both negative and positive feedback effects (*26*, *27*). For example,

$$f(\dot{\theta}) = \varphi(c_p\dot{\theta}) - c_n\dot{\theta} \tag{3}$$

gives positive/negative feedback when the velocity $|\dot{\theta}|$ is small/large as seen in the slope of the vertical isocline (red solid curve) in Fig. 2C, where φ is a function of angular velocity and $\varphi(c_p\dot{\theta})$ is exemplified by $\tanh(c_p\dot{\theta})$. The positive slope near $(\dot{\theta}, \theta) = (0, 0)$ makes the equilibrium point unstable so that the state trajectory diverges, whereas the isocline has a negative slope when $(\dot{\theta}, \theta)$ is away from the origin, leading the trajectory to move toward the origin. Combining these two effects, the trajectory forms a periodic orbit as a stable limit cycle. The mathematical form of the applied nonlinear torque $f(\dot{\theta})$ can differ from that of Eq. 3, which is discussed in detail for specific soft robotic systems in the following sections.

Key factors for nonlinear time-lag feedback

The nonlinear feedback $f(\dot{\theta})$ in Eq. 1 achieves stable oscillation by adjusting the applied torque u on the basis of the angular velocity $\dot{\theta}$. The mechanism of the nonlinear velocity feedback can be essentially achieved by position feedback in nonlinear integral feedback (*28*, *29*). The idea is based on the observation that when the angle oscillates sinusoidally, $\theta = \sin(\omega t)$, the angular velocity $\dot{\theta}$ is proportional to the angle integral q,

$$\theta = \sin(\omega t) \Rightarrow \dot{\theta} = \omega\cos(\omega t), q \triangleq \int \theta(t)dt = (-1/\omega)\cos(\omega t) \Rightarrow \dot{\theta} = -\omega^2 q \tag{4}$$

Hence, q may act as a (scaled) estimate of $\dot{\theta}$ during the steady state oscillation, which leads to the nonlinear integral feedback

$$\ddot{\theta} + c_n\dot{\theta} + \theta = u, \;\; u = \varphi(-\alpha q), \;\; \dot{q} = \theta \tag{5}$$

where $\alpha > 0$ is the strength of the feedback. This system gives a stable limit cycle oscillation similar to Fig. 2C when $\alpha = \omega_2 c_p$ where ω is the oscillation frequency.

Nonlinear time-lag feedback is a variation of the integral feedback given by

$$\ddot{\theta} + c_n\dot{\theta} + \theta = u, \begin{cases} u = -\alpha p \\ p + \tau\dot{p} = \varphi(\theta) \end{cases} \quad (6)$$

where $\tau > 0$ is a time constant. Note that p follows $\varphi(\theta)$ with a time lag τ, and $-\tau\omega^2 p$ converges to the time derivative of $\varphi(\theta)$ when $\varphi(\theta) = \sin(\omega t)$, provided $\tau\omega \gg 1$. The pendulum with the time-lag feedback also has a stable limit cycle qualitatively similar to Fig. 2C. The system behavior under the nonlinear time-lag feedback is determined by two key parameters—the feedback strength (α) and the time lag (τ). The pendulum oscillates in the steady state if the effect of the nonlinear feedback $-\alpha p$ is large enough to overcome the inherent mechanical damping $c_n\dot{\theta}$ and make the equilibrium unstable, which occurs when

$$\alpha\varphi'(0) > c_n^2 + c_n\left(\tau + \frac{1}{\tau}\right) \quad (7)$$

where $\varphi'(0)$ is the derivative of $\varphi(\theta)$ at $\theta = 0$. Generally, the oscillation occurs when the feedback is sufficiently strong, with the required strength increasing as the time lag becomes larger. In short, appropriate feedback strength and time lag would be crucial for enabling steady oscillation. We further discuss the implications of these factors for real-life API systems in the following sections.

Case study with nonlinear time-lag feedback for API

To gain a deeper understanding of nonlinear time-lag feedback in realistic robotic designs, we present a case study from the L. Jin group here—a single–degree-of-freedom mass-spring-damper system to describe the photodriven self-excited oscillation of hydrogels as a typical API system (*20*, *30*). The model below includes the interaction between structural responses (deflection x, velocity $\dot{x}$, and acceleration $\ddot{x}$) and external stimulus (applied force F), which is commonly inherent in API systems (*31*)

$$\begin{aligned} &m\ddot{x} + \beta\dot{x} + kx = F \\ &F + \gamma\dot{F} = -F_\infty |x| / x \end{aligned} \quad (8)$$

where m represents the mass, β is the damping factor, k denotes the stiffness, F_∞ is an excitation force constant, and γ is a characteristic timescale, featuring the solvent diffusion in and out of the hydrogel. Notably, the position- and time-dependent nonlinear excitation $F(x, t)$ is introduced to simulate the alternating irradiation on the hydrogel oscillator during its periodic swelling and deswelling. By defining the correspondence

$$\theta \triangleq x,\ u \triangleq \frac{F}{k},\ \omega_n \triangleq \sqrt{k/m},\ c_n \triangleq \frac{\beta}{m\omega_n},\ p \triangleq -\frac{F}{F_\infty},\ \tau \triangleq \omega_n\gamma,\ \alpha \triangleq \frac{F_\infty}{k} \quad (9)$$

Eq. 8 can be rewritten as

$$\theta'' + c_n\theta' + \theta = u, \begin{cases} u = -\alpha p \\ p + \tau p' = \varphi(x) \end{cases} \quad (10)$$

which shares a similar mathematical form with the previously discussed nonlinear time-lag pendulum model in Eq. 6. Here, $\theta' \triangleq \frac{d\theta}{d\hat{t}} = \frac{1}{\omega_n}\frac{d\theta}{dt} = \frac{1}{\omega_n}\dot{\theta}$, $\theta^{\varepsilon} \triangleq \frac{1}{\omega_n{}^2}\ddot{\theta}$, $\hat{t} \triangleq \omega_n t$, $p' \triangleq \frac{1}{\omega_n}\dot{p}$, $\varphi(x) = |x| / x$. The feedback gain α is essentially the strength of the nonlinear negative damping on the system, as discussed in the previous section. In cases of no or negligible damping (normalized damping factor $c_n = 0$) and when the inertia timescale $\sqrt{m/k}$ is comparable to the excitation timescale γ (i.e., $\tau = 1$), the oscillation amplitude increases as a function of time, and the trajectory on the phase plane diverges away from the initial position, exhibiting the trajectory characteristics of positive feedback shown in Fig. 2B. With a positive normalized damping factor ($c_n > 0$), the trajectory on the phase plane converges to a stable limit cycle, resembling the trajectory of nonlinear feedback systems as shown in Fig. 2C. In this state, the self-excited system oscillates with a steady amplitude.

Toward modeling and designing real-world API systems

It is noteworthy that the above analysis is a simplified model that serves as a good phenomenological approximation to understand the real system. However, it offers limited insight into the actual physical processes (e.g., photothermal-mechanical coupling and water diffusion) occurring in the actuator that influence the time lag and nonlinear isocline as discussed above. To better capture the characteristics of complex real-world systems addressing different material properties, geometries, and actuation mechanisms, we herein propose a more general modeling methodology consisting of a structural model (e.g., Euler-Bernoulli beam, thin plate theory, or continuum elasticity model), a stimulus-structure coupling (e.g., thermomechanical coupling or hygroscopic interaction), and a kinetic law for the stimulus/field variable (e.g., heat transfer for temperature field, diffusion for chemical or humidity stimuli). For the hydrogel case in the last section, which undergoes reversible volumetric changes upon exposure to light by uptaking or expelling the solvent (*20*), such methodology can be applied as follows.

First, the selection of a structural model should be based on the characteristics of structural geometry and deformation mode. In the case of the self-oscillating hydrogel discussed in the last section (*30*), a structural model was chosen on the basis of Euler-Bernoulli beam theory with one fixed end and one free end boundary conditions, suggesting that the hydrogel cantilever with structural deflection $w(x,t)$ along coordinate x is governed by the equation

$$\rho A\frac{\partial^2 w}{\partial t^2} + c\frac{\partial w}{\partial t} + EI\frac{\partial^4 w}{\partial x^4} = EI\frac{\partial^2\left(1/R_{inel}\right)}{\partial x^2} \quad (11)$$

where ρ is the density, A is the cross-sectional area, c is the damping coefficient, E is Young's modulus, I is the area moment of inertia, and R_{inel} is the spontaneous radius of curvature. Meanwhile, the selection of structural models is not unique because a general continuum elasticity model without any structural assumptions (such as small deformation, cross section remains plane, and negligible shear deformation) can also simulate photodriven hydrogel oscillators. Consequently, for other actuators with different geometries and mode shapes, appropriate structural models should be selected.

Second, stimulus-structure coupling is analyzed to correlate the stimulus with the stress or strain in the actuating system. In the same example, the coupling between water concentration $C(z)$ and inelastic strain $\varepsilon_{inel}(z)$ inside the hydrogel can be expressed as

$$1/R_{inel} = -\int_A \varepsilon_{inel}(z) z dA / I$$

where

$$\varepsilon_{inel}(z) = \frac{1}{3}\left(\frac{\Omega C(z) + 1}{\Omega C_0 + 1} - 1\right) \quad (12)$$

Equation 12 is based on the assumption of isotropic deformation and molecular incompressibility, where Ω is the volume of one water molecule, z is the coordinate in the thickness direction, and C_0 is the water concentration in the hydrogel when the hydrogel is in equilibrium with water without irradiation. For different actuators excited by different stimuli, the expression of inelastic strain (e.g., hygroscopic strain and thermal strain) could have specific forms.

Third, for different stimulus fields (e.g., temperature), different kinetic laws should be selected. For this example, kinetic law for water migration can be written as

$$\frac{\partial C}{\partial t} = \frac{D}{k_B T}\frac{\partial}{\partial z}\left(\frac{C}{\lambda_z^2}\frac{\partial \mu}{\partial z}\right) \tag{13}$$

where D is the diffusivity, k_B is the Boltzmann constant, and T is the temperature. According to Eq. 13, the water migration process is driven by the chemical potential gradient, $\partial\mu/\partial z$, and the migration rate is dependent on the deformation ratio λ_z (pore size) of the hydrogel.

Similar analysis could be extended to other stimulus-responsive materials with the potential to construct such nonlinear time-lag feedback. Like hydrogels, liquid crystal polymers (LCPs) are powerful candidates for achieving API because of their hyperelasticity and large deformation capabilities (*32*). For LCPs, shape morphing is triggered upon the reorientation of mesogen via light, heat, or solvent. Among such LCP-based robots, the photoinduced oscillation of azobenzene-functionalized LCP is an exemplar feedback system where power, control, and stimulus response are intricately coupled (*33*). This photoactuation mechanism is enabled by the light-absorptive nature of azobenzene, facilitating the conversion of light energy into chemical (photoisomerization) and thermal products. In this scenario of a vibrating LCP beam, where the top and bottom layers of the beam are alternately illuminated by light (*34*), the structure is similar to the photodriven self-oscillating hydrogel above. Thus, the Euler-Bernoulli beam model in Eq. 11 still works for this case. However, the distinct material properties and actuation mechanisms of LCPs necessitate a population dynamics model as the kinetics law (*35*), in contrast with the chemical gradient–driven diffusion model used for hydrogels. Specifically, the number fraction of cis isomers $\phi(z, t)$ in an LCP is determined by

$$\frac{\partial \phi}{\partial t} = \eta_0 I(1-\phi) - T_0^{-1}\phi \tag{14}$$

where T_0 is the thermal relaxation time of the cis-to-trans state, η_0 is a light-adsorption constant, and $I(z)$ is the light intensity that decays exponentially with the penetration depth (*36*). The inelastic strain in Eq. 12 would be expressed as

$$\varepsilon_{inel}(z, t) = -\xi\phi(z, t) \tag{15}$$

where ξ is the contraction coefficient. Numerous design variables have been explored to tune the feedback strength and the time lag, including azobenzene concentration, crosslink density, and degree of orientation (*37*). For instance, a higher loss modulus delays the mechanical response, leading to higher damping strength and longer time lag. On the other hand, enhancing photothermal efficiency accelerates energy accumulation to reduce time lag (*21*).

Another example is a hygroscopic polymer film in a chamber with a large humidity gradient, which performs autonomous reconfiguration, oscillation, and locomotion on the basis of the expansion/contraction upon moisture absorption/desorption (*38*). In this case, the Euler-Bernoulli beam structural model is not suitable for describing the large deformation and multimodal behavior; instead, finite deformation theory should be used, where the deformation gradient tensor $\mathbf{F}$ can be decomposed into elastic ($\mathbf{F}_{el}$) and inelastic ($\mathbf{F}_{inel}$) contributions

$$\mathbf{F} = \mathbf{F}_{el}\mathbf{F}_{inel} \tag{16}$$

The inelastic strain can be expressed by a linear relationship as

$$\varepsilon_{inel}(x, t) = \psi\left[C(x, t) - C_{ref}\right] \tag{17}$$

where ψ is the coefficient of hygroscopic swelling, quantifying the reconfiguration of hygroscopic polymers in response to concentration C change. C_{ref} is the strain reference concentration. The kinetic law of water molecules is given by

$$\frac{\partial C(x, t)}{\partial t} = \nabla \cdot [D\nabla C(x, t)] \tag{18}$$

In summary, material-based models offer a more realistic and effective approach to capturing the dynamics of API systems. The key challenge lies in accurately modeling the coupling between the structure and external stimuli, reflecting the intricate interactions between the material and the environment. Given that there is no unified model capable of governing all API systems because actuation mechanisms, material properties, and external stimuli vary by situation, the selection of each modeling component must be precise and tailored to the specific system.

EVOLUTION OF PHYSICAL INTELLIGENCE–ENABLED ROBOTS

We observe that the incorporation of nonlinear time-lag feedback to achieve a higher level of autonomy is emerging as a trend in physically intelligent robots, akin to the advancements in the control mechanisms for conventional robots: It has progressed from manual control to preprogrammed responses capable of handling a limited number of scenarios, ultimately advancing to machine learning for the highest level of autonomy (*39*). Such a trend is evidenced in the manipulation of external stimuli across four stages in soft robots: manually controlled stimuli, requiring human intervention; preprogrammed periodic stimuli, free from additional intervention after initiation; cyclic natural stimuli, which leverage environmental fluctuations without human input; and constant stimuli, characterized by self-continuous motion under constant conditions. Among them, the first three stages, which embody physical intelligence for on/off switches, are built on negative feedback loops damping to the equilibrium, whereas the last stage uses nonlinear time-lag feedback to control the most advanced stage for API.

Conventional robots

Conventional robots are predominantly constructed from passive materials such as metal and hard plastics, necessitating manual control to manipulate their movements and actions in their rudimentary stage. In contrast, autonomous rigid robots use processors to navigate various environments and perform tasks. An example is Spot, the quadruped developed by Boston Dynamics (Fig. 3A) (*40*), a successful integration of sophisticated algorithms with rigid body mechanics to traverse diverse terrains. Such robots typically consist of rigid body segments connected by actuated joints, with each segment equipped with its own circuitry. For example, the lamprey-like robot AgnathaX is composed of 10 servomotors, a computer, batteries,

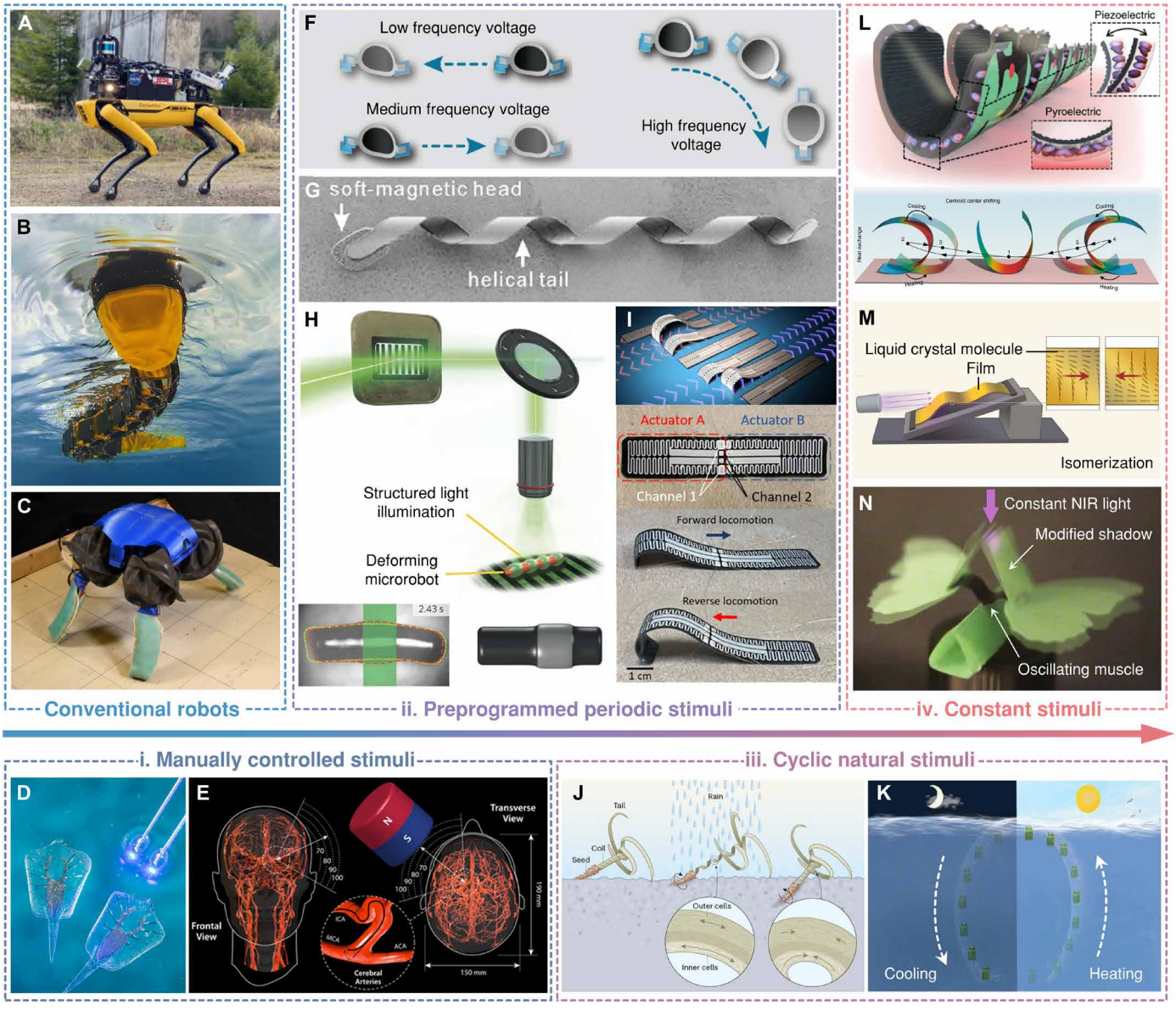

Fig. 3. Evolution of conventional robots and soft robots with an increasing level of autonomy. This evolution starts from (**A** to **C**) conventional robots (*2, 40, 42*) to robots operating under (**D** and **E**) manually controlled stimuli (*10, 46*), (**F** to **I**) preprogrammed periodic stimuli (*47–49, 51*), (**J** and **K**) cyclic natural stimuli (*52, 53*), and (**L** to **N**) constant stimuli (*21, 54, 61*).

and a passive tail module (Fig. 3B) (*2*). Recent advancements have enabled the development of shape-shifting robots with adaptive control policies using soft materials (*41*), such as the amphibious robotic turtle (ART) (Fig. 3C) (*42*). However, achieving the full potential of adaptive and transient soft bodies necessitates distributed computation (*43*). Ultimately, we foresee notable strides in distributed computation, encompassing both hardware and software perspectives, to shift robots from extrinsic, fixed, and centralized systems toward intrinsic, modular, and distributed architectures. Researchers have introduced soft mechanical computing platforms that use complex dynamic behaviors to perform computation and serve as distributed information processing networks (*44*). Additional distributed soft logic gates using fluidic principles have also been proposed (*45*). However, these mechanical approaches currently lack the logic gate density of traditional electronic computers.

Manually controlled stimuli

Alternatively, stimulus-responsive soft robots can achieve similar intelligence at the material level without any embedded processors. To date, in the most primitive form, the control of stimulus-responsive robots requires substantial human intervention. For instance, a light-responsive stingray robot based on optogenetics requires manual manipulation of light sources to initiate and navigate its motion (Fig. 3D) (*10*). In addition, continuous adjustment of the magnetic field is required to guide magnetic robots, particularly in complex surgeries necessitating high precision and untethered

control, such as steering through the tortuous cerebral arteries in endovascular neurosurgery (Fig. 3E) (*46*).

Preprogrammed periodic stimuli

Computerized control of stimuli liberates researchers from the laborious task of manually adjusting the position, direction, and intensity of stimuli for repetitive tasks. For instance, an alternating electric field can power the repeated zipping/unzipping of a dielectric elastomer actuator (Fig. 3F) (*47*); a rotating magnetic field can propel a spiral magnetic actuator forward (Fig. 3G) (*48*); pulsed/structured light can induce crawling in liquid crystal elastomer–based microrobots (Fig. 3H) (*49, 50*); and programmed Joule heating can enable caterpillar-like locomotion to overcome obstacles (Fig. 3I) (*51*). In these designs, preprogramming the periodic stimuli allows for easy alteration of gaits or motion modes on demand.

Cyclic natural stimuli

Naturally occurring stimuli, such as sunlight, humidity, and temperature, have periodic circadian and seasonal variations, offering opportunities that eliminate the need to manually change external stimuli. By definition, robots powered by natural stimuli are considered autonomous despite requiring varying stimulus fields within fixed periodicities. Recently, an *Erodium* seed–inspired self-burying seeding robot was developed on the basis of circadian humidity changes (Fig. 3J) (*52*), and a thermal-responsive hydrogel-based robot was designed to float periodically in response to temperature variations between night and day (Fig. 3K) (*53*).

Constant stimuli

In the recent decade, there has been growing progress in developing self-continuous robots capable of performing tasks under constant stimuli through a built-in nonlinear time-lag feedback loop. This mechanism enables the conversion of constant input into a stable limit cycle oscillation. Various self-continuous motions have been extended to interdisciplinary fields, including self-continuous tumbling and oscillation for electricity generation (Fig. 3L) (*54*–*58*), photonic applications (*59, 60*), undulatory locomotion (Fig. 3M) (*21, 61, 62*), and oscillatory flapping (Fig. 3N) (*20*, *21*, *33*, *63*). Similar feedback loops for API can be realized by meticulously engineering materials and structures via various mechanisms, which are elucidated in the next section.

API FOR AUTONOMOUS SOFT ROBOTS

The self-continuous motion of soft robots involves three fundamental components: the robotic system, the external environment, and the material-environment interactions. Creating such motion requires modulating spatiotemporal changes in any of these three components through the incorporation of systematic instability, inducing spontaneous oscillation in environments, and coupling the macroscopic deformation of the robot with its reception of the stimulus field. As discussed in the "Toward modeling and designing real-world API systems" section, different strategies could be applied to each robotic system under certain environmental stimuli.

Strategies to create self-continuous motion

Gradient/directional stimuli

When a stimulus-responsive material system is subjected to a constant gradient or directional stimulus field, its macroscopic deformation can be coupled with a nonlinear response to the external stimulus. Specifically, upon exposure to the stimulus, the material triggers a deformation to move, either partially or wholly, toward areas where the stimulus is weaker and less efficient. This movement generates a restorative force that resets the system state, exposing the material to stronger stimuli again and thus perpetuating the motion of the system. As a result, the system is subject to a spatiotemporally varying excitation force, as discussed in the "Case study with nonlinear time-lag feedback for API" section, although with potentially different mathematical forms of motion and coupling equations. This strategy is viable and has been extensively investigated because a thermal or humidity gradient can be feasibly established to power self-sustained motion using a heat source or water reservoir across various materials. Temperature gradients, for example, can induce rolling, tumbling, vertical oscillation, and other complex periodic motions in thermotropic liquid crystal elastomers via phase transition (*64*–*66*) or coefficient of thermal expansion materials via nonuniform thermal expansion (*54, 67*), by having the materials move periodically into regions with high/low temperatures (Fig. 4A). For example, prestrained polymer toroidal fibers made from either polydimethylsiloxane (PDMS) or nylon exhibit self-rotation when placed on a hot plate, given that a torque is generated around the fiber's axis because of thermal-induced strain at the contact interface maintained by the external heat source (*67*).

Similarly, humidity-responsive materials can swell and deform under humid conditions, driving cyclic motion into and out of humid regions (Fig. 4B) (*68*–*71*). In addition, a concentration gradient of chemical species, such as pH or organic solvents, can cause the (de)swelling behavior of a swollen gel. This changes the exposure area to the stimuli and thus the (de)swelling kinetics across the gradient, generating periodic motions such as snapping or undulation (Fig. 4C) (*72*–*74*). However, in these cases, high-resolution spatiotemporal control of the stimuli gradient is usually challenging because of the complex energy or mass transport in the surrounding environment. By comparison, light emerges as a more convenient stimulus with the possibility of precisely controlling beam size, directionality, intensity, wavelength, and polarity. Photoresponsive materials can achieve similar motions under light fields with directionality, gradient intensity, or gradient wavelength, via photothermal or photochemical mechanisms (*60, 75*). In such cases, light as a directional stimulus can cause a self-shadowing effect, using the limited light penetration of the photoresponsive material or a passive component to induce a nonlinear photomechanical response (Fig. 4D) (*61, 63, 76*). For instance, the Broer group has developed a Hamiltonian-based model for the photoactuation of a liquid crystal network film, where the degree of mesogen alignment is disrupted under illumination, causing shrinkage along the mesogen alignment, and increases when shadowed (*61*). When exposed to horizontal light, the top surface of the film contracts, creating a bump that moves away from the light until it arrests at the clamped end, where a new crest forms to the left. As the new crest grows, it shadows and eliminates the old crest through a snap-through transition, repeating the process, thus demonstrating nonlinear feedback generating wave propagation. The time lag is determined by the relaxation time of azobenzene. Similarly, a nonlinear feedback–controlled system of two coupled hydrogels driven by constant light was modeled using a heat transfer module, achieving stable homeostatic temperature oscillation via a thermally coupled delay with intelligent self-regulatory behavior (*77*).

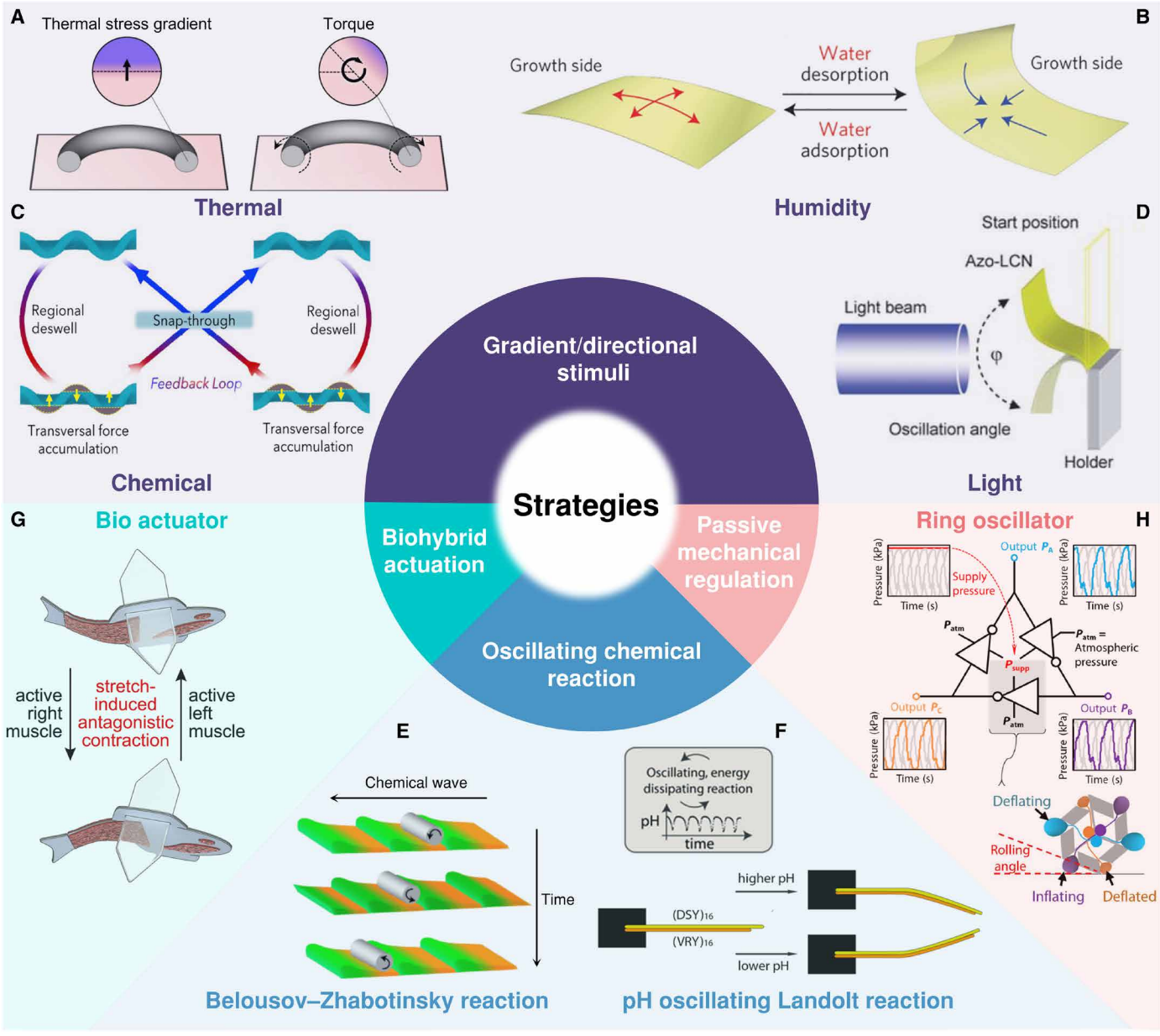

Fig. 4. Strategies to create self-continuous motions. These include building environments with (**A** to **D**) gradient/directional stimuli (*63, 67, 68, 72*), (**E** and **F**) oscillating chemical reactions (*79, 80*), (**G**) biohybrid actuation (*83*), and (**H**) passive mechanical regulation (*91*).

Oscillating chemical reaction

Oscillating chemical reactions can generate periodic changes in chemical stimuli when sufficient reactants are present. Unlike chemically driven robots operating under a constant stimulus field, the chemical environment in these systems autonomously oscillates to sustain the motion. To date, only hydrogel actuators have been reported to use such a mechanism because fast mass exchange between the bulk material and the aqueous environment is required. For example, the Belousov-Zhabotinsky reaction—a classic tricarboxylic acid cycle involving organic acids (such as citric acid or malonic acid), an oxidizing agent, and a metal catalyst—has been used to construct robots with self-continuous motion (*78*). The cyclic redox changes in the catalyst embedded in the hydrogel lead to periodic swelling-deswelling, constructing a stable limit cycle (Fig. 4E). This behavior arises because the lower critical solution temperature of the polymer gel is higher in the oxidized Ru(III) state than in the reduced Ru(II) state, such that the volume of the gel varies spatiotemporally with the oxidation state of Ru because of the change in hydrophilicity (*79*). As the reaction proceeds, the profile of Ru species forms a wave pattern that propagates along the gel, inducing local swelling that creates peaks and creases that move in a peristaltic manner. Propagation of the coupled chemical and mechanical wave is thus able to propel an object placed in the creases by rotating in one direction. Moreover, the pH-oscillating Landolt reaction is

based on a bromate/sulfite/ferrocyanide reaction system where pH oscillates between pH 4.0 and 7.9 with an average period of about 20 min. In such environments, pH-responsive hydrogels can achieve autonomous oscillation and locomotion (Fig. 4F) (*80*). However, constrained by the reaction kinetics, the actuation speed and stroke of these hydrogels are typically limited.

Biohybrid actuation

Biohybrid actuators represent a fascinating intersection of biology and engineering, merging living cells and tissues with artificial components to create dynamic, functional and responsive systems that are especially promising for biomedical applications. These actuators leverage the chemical powering, sensing, taxis, and actuation capabilities of biological cells [e.g., bacteria, algae (*81*)] and tissues [e.g., cardiomyocytes, dorsal and vessel tissues (*82*)]. For instance, a beating heart is a self-oscillating actuator regulated by the electric potential in the sinoatrial node. By exploiting the mechanoelectrical signaling and automaticity of cardiomyocytes, it is possible to construct a biohybrid fish that performs body-caudal fin swimming via reciprocal contraction and relaxation in a muscular bilayer, which can be either light-induced or self-sustained (Fig. 4G) (*83*).

Passive mechanical regulation

Mechanical morphological design can embed control logic directly into the body, thereby reducing reliance on external manipulation and enabling environmental adaptation. An example in nature is the passive propulsion of a dead trout behind an obstacle, where its flexible body resonates with incoming vortices, extracting mechanical energy from the flow to sustain motion (*84*). Such morphology-based passive regulation has been widely demonstrated in hard robotics. For instance, passive dynamic walkers have achieved continuous downhill locomotion solely under gravitational power, without the need for active joint control (*85*–*87*). Another iconic example is the wind-powered Strandbeest, which walks continuously and can autonomously sense changes in terrain, triggering a reversal in direction when approaching the sea or an obstacle (*88*). In soft robotics, similar principles of passive mechanical regulation have been applied to generate continuous motion. For example, plants with wind-dispersed seeds like *Tristellateia* have evolved seed shapes that inherently exhibit aerodynamic stability for long-distance dispersal (*89*). Inspired by such morphology, three-dimensional (3D) microfliers have been developed to autonomously regulate rotational kinematics and minimize falling velocity because their geometries create high drag forces during freefall (*90*). Moreover, fluidic circuits leverage soft pneumatic or hydraulic bistable valves to produce periodic, temporally coordinated output pressures from a single constant-pressure source. These circuits replicate digital logic entirely within soft systems to generate autonomous, self-sustained motion. For example, a pneumatic ring oscillator constructed using an odd number of bistable valves connected in a loop creates a system-level instability that drives sequential oscillation between high- and low-pressure states. By harnessing the nonlinear mechanical behavior in elastomeric materials, ring oscillators can generate complex behaviors, such as undulating and rolling motions in soft robots, without the need for hard valves or electronic controls (Fig. 4H) (*91*–*94*). Recently, a monolithic 3D-printable pneumatic walking robot has been reported, using a four-phase bistable oscillating valve to generate autonomous amphibious and terrain-adaptive walking with an onboard air supply (*95*).

Self-continuous locomotion

All locomotion in soft robots is generated by the displacement of the center of mass triggered by the actuator, and this process relies on the transition from intrinsic structural asymmetry to nonreciprocal interactions with the environment (*4*). Robots based entirely on soft materials can theoretically have unlimited degrees of freedom, enabling a complexity of motion and mechanical compliance that is unattainable through conventional robots. For example, a ferromagnetic robot with magnetic particles embedded in a soft matrix demonstrates omnidirectional steering, enabling navigation through complex and constrained environments like a cerebrovascular phantom (*46*). Moreover, basic deformations (e.g., linear deformation, bending, and torsion) can be coupled to produce multimodal actuation, free from the geometric constraints of anchors (*6*).

Different locomotion modes in organisms arise from their interactions with the environment, which may vary according to their specific surroundings. Therefore, in this section, we categorize bionic autonomous self-continuous soft robots on the basis of their working environments: terrestrial, aquatic, and aerial locomotion. In addition, soft robots that have multimodal locomotion capability in diverse terrains and environments have been proposed to demonstrate environmental adaptability, much like many organisms that adjust their locomotion modes in response to changing environments. Meanwhile, we also summarize some theoretical designs that may be realized in the future, providing inspiration for further developments in this field.

Terrestrial locomotion

Terrestrial locomotion in soft robots is a fundamental and widely explored area in robotics because of its direct relevance and applicability to human life. For soft robots, time-varying shapes are essential for effective interaction with the substrate, which ensures appropriate friction for continuous movement (*8*). These robots can mimic vertebrate-like legged walking or crawling, driven by constant stimuli. Untethered from power and control units, they can be miniaturized to insect-sized forms, such as the 88-mg autonomous walking robot capable of carrying payloads across outdoor surfaces through catalytic combustion regulated by cyclic activation of shape memory alloy shutters (Fig. 5A) (*96*). Structural asymmetry converts such stable oscillations into nonreciprocal legged walking at the millimeter scale, powered by various types of stimuli, including light (*97*), humidity (*71*), bioenergy (*98*), and chemicals (*99*) (Fig. 5B). In addition, some robots can exhibit an undulatory gait akin to worms, with devices like a bilayer oscillator powered by sunlight (Fig. 5C) (*21, 61*).

Self-excited oscillation can also enable rotary locomotion, facilitated by toroidal, twisting, or helical geometries that produce asymmetric interactions with the surroundings in zero–elastic-energy modes. In such systems, the time lag is governed by the characteristic thermal relaxation time, and the excitation force is related to the temperature difference between a heat source and the environment (*67, 100*). In ring-shaped structures with internal prestress (Fig. 5D), the asymmetric stimuli from the bottom trigger the snapping to create instability that causes the structure to cyclically flip between stable states, driven by the synergistic effect of friction and gravity (*101*). Moreover, introducing a desired defect into the above ring can harness periodic symmetry breaking of tangential driving forces, enabling motion modes like spinning and orbiting (*102*). Meanwhile, by using advanced fabrication techniques (e.g., origami and kirigami), the initial structure of these robots can be noncircular, allowing for shape adaptation to stimuli and transforming 2D shapes to a 3D rolling state (*103*). Cylinders and twisted ribbons are commonly used as rolling structures because of their relatively accessible fabrication processes (*64*). Interestingly, they can mimic the

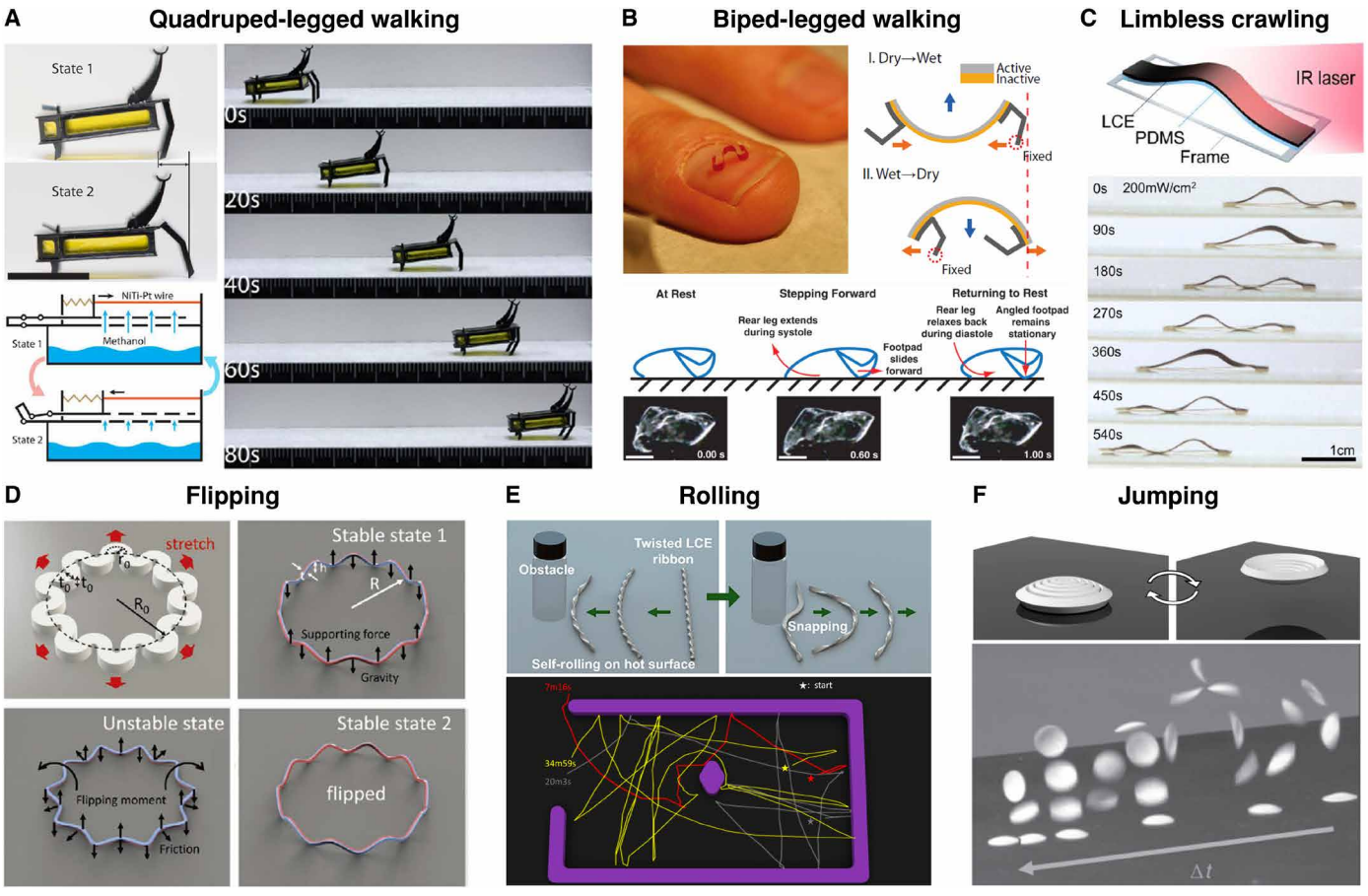

Fig. 5. Terrestrial locomotion of autonomous soft robots with different motion modes. These include (**A**) quadruped-legged walking (*96*), (**B**) biped-legged walking (*71*, *97*, *98*), (**C**) limbless crawling (*21*), (**D**) flipping (*101*), (**E**) rolling (*104*), and (**F**) jumping (*74*).

obstacle avoidance behavior of real organisms—when encountering obstacles, they sense the contact force and adaptively perform a snap-back motion to move in the opposite direction, showcasing their intelligence for maze escaping and possible extension to unstructured real-world terrains (Fig. 5E) (*104*).

Furthermore, jumping in soft robots necessitates a rapid energy release to generate sufficient lift force to overcome gravity, which is often achieved via a snap-through buckling process with accumulated elastic energy. This energy accumulation can be realized using the deswelling of elastomer swollen in organic solvent (Fig. 5F) (*74*). Because of the shape inversion during the snap-through process, a spontaneous resetting mechanism is necessary to complete a closed loop for continuous jumping. Similarly, photothermal mechanisms can be used to achieve autonomous multimodal terrestrial locomotion, where variations in surface adhesion modulate energy accumulation and morphological transitions, enabling the robot to adaptively switch between self-sustained rolling and jumping across different environments (*105*).

Aquatic locomotion

Unlike terrestrial locomotion, movement through aquatic environments involves contact with all surfaces, resulting in larger drag forces. In nature, organisms select swimming modes on the basis of their body parameters, including shape and size, which influence their interaction with the fluid environment, characterized by the Reynolds number (*106*).

Microorganisms (e.g., bacteria) and slender-bodied fish (e.g., eels, rays) often exist in viscous-dominated environments, where they move nonreciprocally by generating traveling waves as undulations. Similarly, soft robots with microscale or slender structures often use undulation for self-sustained locomotion. For example, a monolithic liquid crystal gel constrained in a frame can propel itself via undulatory motion on the substrate, with its propulsion direction controlled by the programmed incidence angle of light as horizontal and vertical illumination triggers distinct morphological transformations that induce undulating in opposite directions (Fig. 6A) (*62*). Meanwhile, programmed light patterns can adjust wavy morphologies to enable tunable cargo transportation (*107*). Besides, asymmetric irradiation angled in both axial and radial directions can induce a sperm-like swirling motion if the slender body can generate forces in orthogonal directions (*108*).

In contrast, larger-sized organisms (e.g., sharks, tuna, and dolphins) typically use fins or flukes—limited parts of their entire bodies—to generate symmetric oscillations with sufficient force to remain under inertia-dominated conditions. Similarly, soft robotic swimmers with higher structural stiffness use oscillatory locomotion via a built-in self-shadowing mechanism under constant light (Fig. 6B, top) (*20*). Furthermore, introducing a second light source

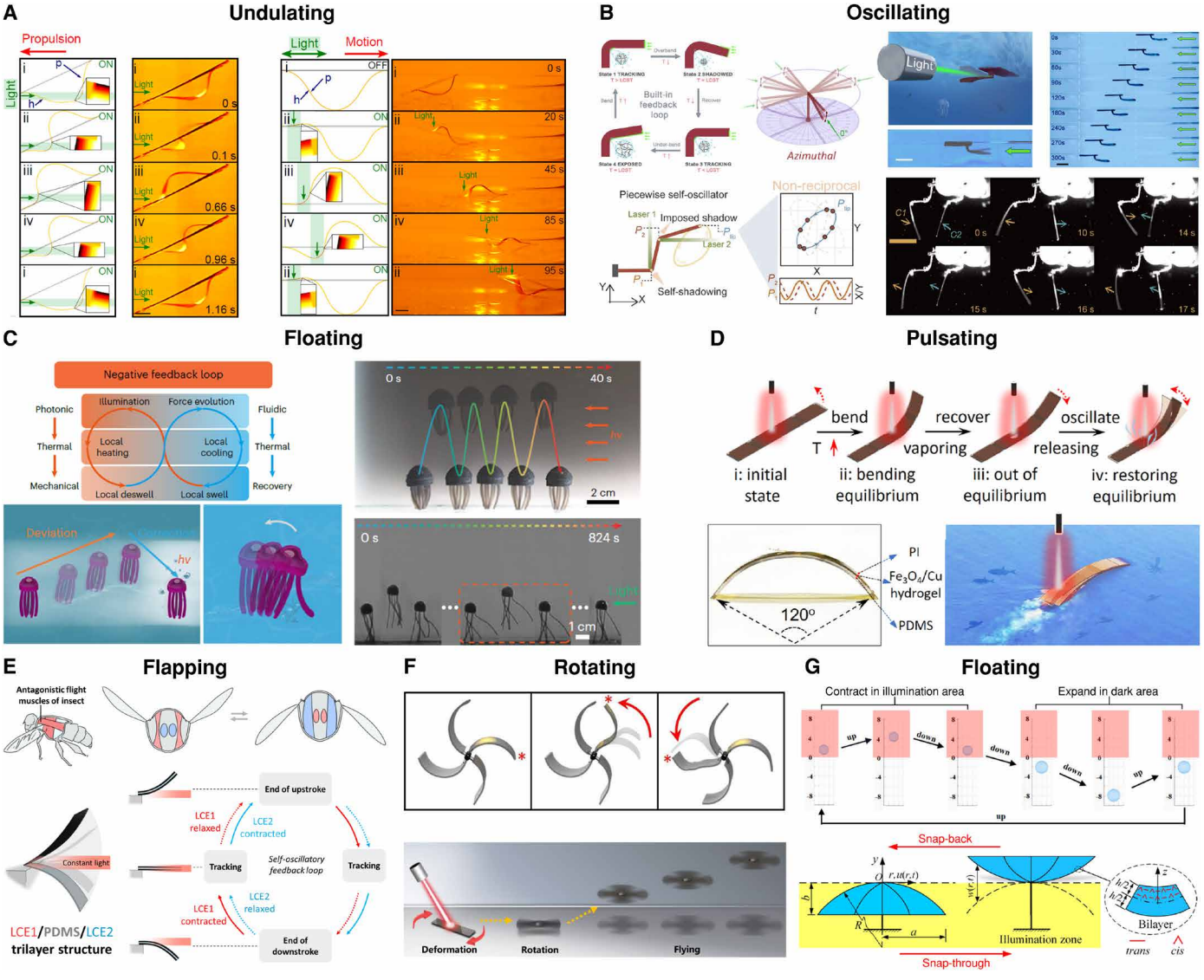

Fig. 6. Aquatic locomotion of autonomous soft robots with different motion modes. (**A**) Undulating (*62*), (**B**) oscillating (*20, 109*), (**C**) floating (*53*), and (**D**) pulsating (*111*) robots. Potential mechanisms to achieve aerial locomotion in autonomous soft robots: (**E**) flapping (*31*), (**F**) rotating (*113, 114*), and (**G**) floating (*115, 116*) mechanisms.

orthogonally can convert the reciprocal oscillation into nonreciprocal motion, enhancing the possibility of generating vortices for fluid transportation (Fig. 6B, bottom) (*109*) and allowing a collective synchronization between two oscillators (*110*).

Some organisms (e.g., jellyfish) can regulate their floating depth in response to periodic changes in their habitats, such as temperature or light variations throughout the day. This environmental adaptation can be replicated in photothermal hydrogel-based robots to complete a periodic floating cycle via dual-responsive swelling/deswelling self-regulation (Fig. 6C) (*53*). This mechanism, based on localized shape morphing propelled by a photothermotactic flow, enables adaptable phototactic locomotion toward a light source with continuously varying angles.

In addition, some organisms (e.g., squid) achieve pulsatile swimming by regularly ingesting and expelling volumes of fluid to propel themselves. This mechanism inspires the design of autonomous soft robots capable of self-continuous periodic liquid or gas generation. Using high-efficiency photothermal agents to generate steam, the neuston-like swimming robot reaches a swimming velocity of 4 body lengths per min (Fig. 6D), providing a performance assessment comparable to those of chordate nekton and neuston (*111*).

Aerial locomotion

Aerial locomotion is the most challenging of all three locomotion types to realize because it requires the actuator to have a high thrust-to-weight ratio to generate sufficient lift force to overcome its own mass (*31*). Although few soft robots have achieved this type of autonomous locomotion without an intricate electronic apparatus, several designs and theoretical models show promise and merit discussion. First, antagonistic muscle pairs, a well-known biological structure, offer a commendable design strategy for achieving high actuation power by facilitating efficient energy accumulation by providing counteracting forces (*112*). On the basis of this strategy, a

flapping active-passive-active trilayer oscillatory robot amplifies power density by 275 times compared with counterparts without antagonistic structures, surpassing the insect muscle threshold of 29 W/kg (Fig. 6E) (*31*). Although its thrust-to-weight ratio is 0.32, falling short of the required 1 for liftoff, the oscillator holds promise for light-powered autonomous aerial vehicles. Second, light-triggered rotation is another viable way to generate continuous lift force, despite the current bottleneck of insufficient output (Fig. 6F, top) (*113*). A recently proposed helicopter-like rotary robot made from hygroscopic agar/silk fibroin and graphene components, fueled by photoinduced jet propulsion, demonstrates potential but is limited by the need to refill water for steam generation (Fig. 6F, bottom) (*114*). Third, some theoretical models demonstrate potential mechanisms for aerial locomotion, such as a photoresponsive balloon (*115*) and a parachute-like shell (*116*) for oscillatory floating under steady illumination (Fig. 6G). The aforementioned designs are noteworthy; however, to realize truly uncrewed soft aerial vehicles, it is essential to optimize at both the material and engineering levels to enhance performance beyond leveraging API. This includes the synthesis of soft actuators with enhanced mechanical robustness, energy efficiency, and actuation performance, along with the integration of advanced aerodynamic architectures to maximize lift generation and maintain stability under varying flight conditions.

Multienvironmental locomotion

Multienvironmental locomotion under changing conditions has been a long-standing focus in robotics development (*117*). As discussed, the interaction between robots and different environments varies substantially in the contacting parts. Therefore, the ability to smoothly switch motion modes adaptively is crucial because external changes may result in uncoordinated dynamics with sudden changes in velocity and acceleration during the transition and potentially irreversible harm to the system. Compared with conventional rigid robots, soft robots benefit from higher degrees of freedom, allowing them to better adjust their shape to adapt to various environmental changes (*6*). Meanwhile, whole-body sensing enables them to continuously detect both expected and unexpected environmental changes from all directions in real time. However, without chip-based algorithms and human intervention, motion switching relies solely on the material identity, posing an inevitable challenge to moving toward a higher level of physical intelligence beyond API with a single motion mode. As a possible solution, structural instability can influence motion modes in response to external changes. For example, with only increasing axial force, an elastic filament can undergo three kinds of motion modes—static standing, 3D spinning, and 2D flapping—across two bifurcation points (*118*), suggesting the feasibility of instability-driven multimodal soft robots with environmental adaptation. Besides, intricate molecular design with multistable phases presents another viable option. For instance, some LCPs capable of transitioning between multiple liquid crystal phases can change their bending direction during unidirectional heating/cooling processes (*119*). Another distinctive opportunity lies in the development of multiresponsive materials with enhanced sensing capabilities, which could manifest as varied output performance from the same input stimuli (e.g., light of different intensities) (*120*) or the combination of disparate stimuli (e.g., heat, light, humidity, and chemical signals) (*121*). A recent report invoking Pavlovian "training" of multistimulus response in soft materials is also motivating for the prospect of integrating responses to noncognitive but multipronged stimuli that emulate mechanisms used in the natural world (*122*).

In addition, combinatorial API and conventional intelligence approaches may offer substantial advantages for multienvironment robots because of the high variability in the environmental variables. The ART exemplifies the concept, featuring morphing limbs that transition between flipper and leg configurations to enable both aquatic and terrestrial locomotion (*42*). Previous methods manually adjusted the ART's limb state and control policies using preprogrammed open-loop strategies and teleoperated transitions. As the ART progresses toward autonomous cross-domain transitions, integrating API concepts with a preprogrammed policy library could enhance efficiency in multienvironment locomotion. For example, humidity-sensitive materials triggering limb-state changes through swelling or pressure-sensitive materials adapting propulsion strategies from drag-based paddling to lift-based flapping on the basis of hydrostatic pressure changes illustrate potential advancements. Distinctive environmental markers and corresponding responsive materials have the potential to streamline multienvironment robotics by reducing the complexity of sensor arrays, electronics, and computational requirements. We believe that such autonomous multimodal soft robots with environmental adaptation will illuminate a pathway for robotics development.

CONCLUSIONS AND PERSPECTIVES

Integrating nonlinear time-lag feedback in soft robots has advanced physical intelligence, enabling autonomous robots to achieve embodied intelligence with multiple locomotion modalities on demand, especially in miniature robots. Nevertheless, we have to admit that achieving biological-level autonomy for real engineering applications remains a distant goal. To bridge this gap, many areas require further investigation.

Scaling up beyond microrobots

API has seen the most rapid development in microrobots, where their small size facilitates the use of local environmental cues and rapid actuation via diffusion-driven mechanisms. However, scaling to macrorobots necessitates overcoming limitations in environmental control and actuation kinetics. Diffusive heat and light fields, large-area stimuli, and oscillatory pneumatic or hydraulic circuits show promise for driving larger robots. Meanwhile, mass production and cost reduction in physical intelligent materials (e.g., LCP and biohybrid actuators) are essential to translate micrometer-scale intelligence to macroscale applications.

Energy use

Another challenge lies in energy efficiency, which also limits scaling up to some extent. Many soft robots, particularly those actuated by light, suffer from low energy use and still rely on high-intensity, continuous inputs unavailable in natural settings. Enhancing energy conversion mechanisms and developing materials with higher power densities are critical to enabling such robots to harvest and convert ambient energy sources (e.g., sunlight, temperature gradients, or humidity flow) into locomotion. This advancement would unlock flight capabilities such as hovering and aerial maneuvering and expand physical intelligent systems beyond thin-film architectures, making them suitable for high-load, agile tasks while preserving safe, compliant interaction with humans.

Collective behavior

Collective or synchronized behavior is crucial for soft robot teams or swarms, offering new capabilities to interact with each other and surrounding environments (*110, 123*). This behavior, inspired by natural phenomena like fish schooling (*124*) or the tube feet of starfish (*125*), could lead to novel applications in self-continuous microarrays for microwalkers, dynamic sensors, cell-culture scaffolds, or information encryption (*126*, *127*). In this context, API entails not only local responsiveness but also the ability to modulate behavior on the basis of neighboring units and shared stimuli, thereby achieving more efficient coverage and functionalities across large areas.

Combination with functionalities

Beyond self-sustained locomotion as a fundamental behavior, other forms of physical intelligence—such as self-healing, degradability, recyclability, shape memory, reconfigurability, smart adhesion, photochromism, and mechanochromism, as well as piezoelectric, ferroelectric, and magnetoelectric responses—are worthy of attention (*5*). These features will further expand the functionality and application of soft robots. Among them, multimodal actuation/locomotion, multistate homeostasis, and multienvironmental adaptability are inevitable steps toward achieving lifelike intelligence to perform multiple motion modes in changing situations, whereas autonomous functions, such as cargo delivery, object manipulation, and color change, can be integrated into such soft robots.

Memory, logic, and decision-making integration

Integrating memory, logical operations, and decision-making into a soft robot is essential for advanced intelligent behavior. Reprogrammable mechanical metamaterials can enable information storage in soft systems (*128*). Mechanical multistable structures and transition (or solitary) waves (*129*, *130*) or fluidic circuits (*45*) can be used to create integrated logic operations in soft robots toward autonomous control, decision-making, and computation.

Modeling

Modeling should support the design of API systems by enabling computational testing of various scenarios and theoretical analyses of emergent behaviors, such as the stability of limit cycles, which may reveal novel mechanisms beyond those driven by nonlinear time-lag feedback. However, developing a unified model to accurately capture the nonlinear, dynamic, and often unpredictable behavior of API systems remains a major hurdle because of the complexity of real-world conditions. Advancements in computational tools like finite element analysis and machine learning are necessary to address the issue of high computational cost and the absence of a standardized modeling framework.

To achieve these goals, advanced fabrication technologies such as origami/kirigami, microfabrication methods (e.g., lithography, etching, and deposition), 3D fabrication (e.g., two-photon polymerization and 3D assembly), and shear-flow–induced alignment demonstrate great promise (*131*, *132*). These technologies enable soft robot designs with hierarchical structures across multiple length scales and will need to be coupled with advanced multiphysics simulation/modeling tools for the optimal design of soft robots with API.

Last, we believe that the future of autonomous soft robots is inherently interdisciplinary because of its complexity. It will require the joint efforts of researchers in chemistry (molecular design), materials science (fabrication for molecular alignment), mechanics (device construction), mathematics (modeling), robotics, and biology (system-level integration) to achieve system-level integration for fully autonomous soft robots. We envision future API-enabled soft robots to be powered by ambient energy and feature multiple integrated functions, including sensing capability, multimodal actuation/locomotion, memory, communication, and decision-making in response to changing environments, while demonstrating collective behaviors in large numbers, bringing them closer to real engineering applications.

REFERENCES AND NOTES

1. E. D. Tytell, J. H. Long, Biorobotic insights into neuromechanical coordination of undulatory swimming. *Sci. Robot.* **6**, eabk0620 (2021).
2. R. Thandiackal, K. Melo, L. Paez, J. Herault, T. Kano, K. Akiyama, F. Boyer, D. Ryczko, A. Ishiguro, A. J. Ijspeert, Emergence of robust self-organized undulatory swimming based on local hydrodynamic force sensing. *Sci. Robot.* **6**, eabf6354 (2021).
3. A. J. Ijspeert, A. Crespi, D. Ryczko, J.-M. Cabelguen, From swimming to walking with a salamander robot driven by a spinal cord model. *Science* **315**, 1416–1420 (2007).
4. C. S. X. Ng, M. W. M. Tan, C. Xu, Z. Yang, P. S. Lee, G. Z. Lum, Locomotion of miniature soft robots. *Adv. Mater.* **33**, 2003558 (2021).
5. M. Sitti, Physical intelligence as a new paradigm. *Extreme Mech. Lett.* **46**, 101340 (2021).
6. D. R. Yao, I. Kim, S. Yin, W. Gao, Multimodal soft robotic actuation and locomotion. *Adv. Mater.* **36**, e2308829 (2024).
7. C. Hegde, J. Su, J. M. R. Tan, K. He, X. Chen, S. Magdassi, Sensing in soft robotics. *ACS Nano* **17**, 15277–15307 (2023).
8. X.-Q. Wang, G. W. Ho, Design of untethered soft material micromachine for life-like locomotion. *Mater. Today* **53**, 197–216 (2022).
9. Y. Jung, K. Kwon, J. Lee, S. H. Ko, Untethered soft actuators for soft standalone robotics. *Nat. Commun.* **15**, 3510 (2024).
10. S.-J. Park, M. Gazzola, K. S. Park, S. Park, V. Di Santo, E. L. Blevins, J. U. Lind, P. H. Campbell, S. Dauth, A. K. Capulli, F. S. Pasqualini, S. Ahn, A. Cho, H. Yuan, B. M. Maoz, R. Vijaykumar, J.-W. Choi, K. Deisseroth, G. V. Lauder, L. Mahadevan, K. K. Parker, Phototactic guidance of a tissue-engineered soft-robotic ray. *Science* **353**, 158–162 (2016).
11. W. Feng, Q. He, L. Zhang, Embedded physical intelligence in liquid crystalline polymer actuators and robots. *Adv. Mater.* **36**, 2312313 (2024).
12. L. C. van Laake, J. T. B. Overvelde, Bio-inspired autonomy in soft robots. *Commun. Mater.* **5**, 198 (2024).
13. J. Wu, O. L. Loucks, From balance of nature to hierarchical patch dynamics: A paradigm shift in ecology. *Q. Rev. Biol.* **70**, 439–466 (1995).
14. A. Jenkins, Self-oscillation. *Phys. Rep.* **525**, 167–222 (2013).
15. J. A. Curry, J. L. Schramm, E. E. Ebert, Sea ice-albedo climate feedback mechanism. *J. Clim.* **8**, 240–247 (1995).
16. J. L. Hargrove, "Positive and negative feedback: Insulin and the use of fatty acids and glucose for energy" in *Dynamic Modeling in the Health Sciences* (Springer, 1998), pp. 255–261.
17. S. J. Cooper, From Claude Bernard to Walter Cannon. Emergence of the concept of homeostasis. *Appetite* **51**, 419–427 (2008).
18. T. Kambiz Arab, M. Augustin, "PID control theory" in *Introduction to PID Controllers: Theory, Tuning, and Application to Frontier Areas*, R. C. Panda, Ed. (IntechOpen, 2012), pp. 213–228.
19. E. S. Zeron, Positive and negative feedback in engineering and biology. *Math. Model. Nat. Phenom.* **3**, 67–84 (2008).
20. Y. Zhao, C. Xuan, X. Qian, Y. Alsaid, M. Hua, L. Jin, X. He, Soft phototactic swimmer based on self-sustained hydrogel oscillator. *Sci. Robot.* **4**, eaax7112 (2019).
21. Y. Zhao, Q. Li, Z. Liu, Y. Alsaid, P. Shi, M. K. Jawed, X. He, Sunlight-powered self-excited oscillators for sustainable autonomous soft robotics. *Sci. Robot.* **8**, eadf4753 (2023).
22. K. J. Åström, R. Murray, *Feedback Systems: An Introduction for Scientists and Engineers* (Princeton Univ. Press, 2021).
23. E. M. Izhikevich, *Dynamical Systems in Neuroscience: The Geometry of Excitability and Bursting* (MIT Press, 2006).
24. Z.-X. Liu, Y.-J. Qian, X.-D. Yang, W. Zhang, Panel flutter mechanism of rectangular solar sails based on traveling mode analysis. *Aerosp. Sci. Technol.* **118**, 107015 (2021).
25. Y.-J. Qian, L.-E. Zuo, Z.-X. Liu, X.-D. Yang, L. Xu, Flutter mechanism analysis for circular solar sail. *AIAA J.* **61**, 497–504 (2023).
26. D. L. Raney, E. C. Slominski, Mechanization and control concepts for biologically inspired micro air vehicles. *J. Aircr.* **41**, 1257–1265 (2004).
27. T. Iwasaki, M. Zheng, Sensory feedback mechanism underlying entrainment of central pattern generator to mechanical resonance. *Biol. Cybern.* **94**, 245–261 (2006).
28. C. A. Williams, S. P. DeWeerth, A comparison of resonance tuning with positive versus negative sensory feedback. *Biol. Cybern.* **96**, 603–614 (2007).

29. Y. Futakata, T. Iwasaki, Formal analysis of resonance entrainment by central pattern generator. *J. Math. Biol.* **57**, 183–207 (2008).
30. C. Xuan, Y. Zhou, Y. Zhao, X. He, L. Jin, Photodriven self-excited hydrogel oscillators. *Phys. Rev. Appl.* **17**, 014007 (2022).
31. Y. Zhao, Z. Liu, P. Shi, C. Chen, Y. Alsaid, Y. Yan, X. He, Antagonistic-contracting high-power photo-oscillators for multifunctional actuations. *Nat. Mater.* **24**, 116–124 (2025).
32. R. Baines, F. Fish, J. Bongard, R. Kramer-Bottiglio, Robots that evolve on demand. *Nat. Rev. Mater.* **9**, 822–835 (2024).
33. T. J. White, N. V. Tabiryan, S. V. Serak, U. A. Hrozhyk, V. P. Tondiglia, H. Koerner, R. A. Vaia, T. J. Bunning, A high frequency photodriven polymer oscillator. *Soft Matter* **4**, 1796–1798 (2008).
34. K. Li, S. Cai, Modeling of light-driven bending vibration of a liquid crystal elastomer beam. *J. Appl. Mech.* **83**, 031009 (2015).
35. P. M. Hogan, A. R. Tajbakhsh, E. M. Terentjev, UV manipulation of order and macroscopic shape in nematic elastomers. *Phys. Rev. E* **65**, 041720 (2002).
36. X. Liang, Z. Chen, L. Zhu, K. Li, Light-powered self-excited oscillation of a liquid crystal elastomer pendulum. *Mech. Syst. Signal Process.* **163**, 108140 (2022).
37. K. M. Lee, M. L. Smith, H. Koerner, N. Tabiryan, R. A. Vaia, T. J. Bunning, T. J. White, Photodriven, flexural–torsional oscillation of glassy azobenzene liquid crystal polymer networks. *Adv. Funct. Mater.* **21**, 2913–2918 (2011).
38. B. E. Treml, R. N. McKenzie, P. Buskohl, D. Wang, M. Kuhn, L.-S. Tan, R. A. Vaia, Autonomous motility of polymer films. *Adv. Mater.* **30**, 1705616 (2018).
39. J. M. Beer, A. D. Fisk, W. A. Rogers, Toward a framework for levels of robot autonomy in human-robot interaction. *J. Hum. Robot Interact.* **3**, 74–99 (2014).
40. A. Bouman, M. F. Ginting, N. Alatur, M. Palieri, D. D. Fan, T. Touma, "Autonomous Spot: Long-range autonomous exploration of extreme environments with legged locomotion," in *2020 IEEE/RSJ International Conference on Intelligent Robots and Systems* (*IROS*) (IEEE, 2020), pp. 2518–2525.
41. D. Shah, B. Yang, S. Kriegman, M. Levin, J. Bongard, R. Kramer-Bottiglio, Shape changing robots: Bioinspiration, simulation, and physical realization. *Adv. Mater.* **33**, e2002882 (2021).
42. R. Baines, S. K. Patiballa, J. Booth, L. Ramirez, T. Sipple, A. Garcia, F. Fish, R. Kramer-Bottiglio, Multi-environment robotic transitions through adaptive morphogenesis. *Nature* **610**, 283–289 (2022).
43. M. A. McEvoy, N. Correll, Materials that couple sensing, actuation, computation, and communication. *Science* **347**, 1261689 (2015).
44. H. Yasuda, P. R. Buskohl, A. Gillman, T. D. Murphey, S. Stepney, R. A. Vaia, J. R. Raney, Mechanical computing. *Nature* **598**, 39–48 (2021).
45. D. J. Preston, P. Rothemund, H. J. Jiang, M. P. Nemitz, J. Rawson, Z. Suo, G. M. Whitesides, Digital logic for soft devices. *Proc. Natl. Acad. Sci. U.S.A.* **116**, 7750–7759 (2019).
46. Y. Kim, E. Genevriere, P. Harker, J. Choe, M. Balicki, R. W. Regenhardt, J. E. Vranic, A. A. Dmytriw, A. B. Patel, X. Zhao, Telerobotic neurovascular interventions with magnetic manipulation. *Sci. Robot.* **7**, eabg9907 (2022).
47. D. Wang, B. Zhao, X. Li, L. Dong, M. Zhang, J. Zou, G. Gu, Dexterous electrical-driven soft robots with reconfigurable chiral-lattice foot design. *Nat. Commun.* **14**, 5067 (2023).
48. L. Zhang, J. J. Abbott, L. Dong, B. E. Kratochvil, D. Bell, B. J. Nelson, Artificial bacterial flagella: Fabrication and magnetic control. *Appl. Phys. Lett.* **94**, 162906 (2009).
49. S. Palagi, A. G. Mark, S. Y. Reigh, K. Melde, T. Qiu, H. Zeng, C. Parmeggiani, D. Martella, A. Sanchez-Castillo, N. Kapernaum, F. Giesselmann, D. S. Wiersma, E. Lauga, P. Fischer, Structured light enables biomimetic swimming and versatile locomotion of photoresponsive soft microrobots. *Nat. Mater.* **15**, 647–653 (2016).
50. H. Zeng, P. Wasylczyk, C. Parmeggiani, D. Martella, M. Burresi, D. S. Wiersma, Light-fueled microscopic walkers. *Adv. Mater.* **27**, 3883–3887 (2015).
51. S. Wu, Y. Hong, Y. Zhao, J. Yin, Y. Zhu, Caterpillar-inspired soft crawling robot with distributed programmable thermal actuation. *Sci. Adv.* **9**, eadf8014 (2023).
52. D. Luo, A. Maheshwari, A. Danielescu, J. Li, Y. Yang, Y. Tao, L. Sun, D. K. Patel, G. Wang, S. Yang, T. Zhang, L. Yao, Autonomous self-burying seed carriers for aerial seeding. *Nature* **614**, 463–470 (2023).
53. G. Hou, X. Zhang, F. Du, Y. Wu, X. Zhang, Z. Lei, W. Lu, F. Zhang, G. Yang, H. Wang, Z. Liu, R. Wang, Q. Ge, J. Chen, G. Meng, N. X. Fang, X. Qian, Self-regulated underwater phototaxis of a photoresponsive hydrogel-based phototactic vehicle. *Nat. Nanotechnol.* **19**, 77–84 (2024).
54. X.-Q. Wang, C. F. Tan, K. H. Chan, X. Lu, L. Zhu, S.-W. Kim, G. W. Ho, In-built thermo-mechanical cooperative feedback mechanism for self-propelled multimodal locomotion and electricity generation. *Nat. Commun.* **9**, 3438 (2018).
55. R. Lan, J. Sun, C. Shen, R. Huang, Z. Zhang, L. Zhang, L. Wang, H. Yang, Near-infrared photodriven self-sustained oscillation of liquid-crystalline network film with predesignated polydopamine coating. *Adv. Mater.* **32**, e1906319 (2020).
56. Q. Wang, Z. Wu, J. Li, J. Wei, J. Guo, M. Yin, Spontaneous and continuous actuators driven by fluctuations in ambient humidity for energy-harvesting applications. *ACS Appl. Mater. Interfaces* **14**, 38972–38980 (2022).
57. Z.-Z. Nie, M. Wang, S. Huang, Z.-Y. Liu, H. Yang, Multimodal self-sustainable autonomous locomotions of light-driven seifert ribbon actuators based on liquid crystal elastomers. *Angew. Chem. Int. Ed. Engl.* **62**, e202304081 (2023).
58. L. Yang, L. Chang, Y. Hu, M. Huang, Q. Ji, P. Lu, J. Liu, W. Chen, Y. Wu, An autonomous soft actuator with light-driven self-sustained wavelike oscillation for phototactic self-locomotion and power generation. *Adv. Funct. Mater.* **30**, 20201908842 (2020).
59. R. Zheng, L. Ma, W. Feng, J. Pan, Z. Wang, Z. Chen, Y. Zhang, C. Li, P. Chen, H. K. Bisoyi, B. Li, Q. Li, Y. Lu, Autonomous self-sustained liquid crystal actuators enabling active photonic applications. *Adv. Funct. Mater.* **33**, 20232301142 (2023).
60. Z. Hu, Y. Li, J. Lv, Phototunable self-oscillating system driven by a self-winding fiber actuator. *Nat. Commun.* **12**, 3211 (2021).
61. A. H. Gelebart, D. J. Mulder, M. Varga, A. Konya, G. Vantomme, E. W. Meijer, R. L. B. Selinger, D. J. Broer, Making waves in a photoactive polymer film. *Nature* **546**, 632–636 (2017).
62. H. Shahsavan, A. Aghakhani, H. Zeng, Y. Guo, Z. S. Davidson, A. Priimagi, M. Sitti, Bioinspired underwater locomotion of light-driven liquid crystal gels. *Proc. Natl. Acad. Sci. U.S.A.* **117**, 5125–5133 (2020).
63. S. Serak, N. Tabiryan, R. Vergara, T. J. White, R. A. Vaia, T. J. Bunning, Liquid crystalline polymer cantilever oscillators fueled by light. *Soft Matter* **6**, 779–783 (2010).
64. C. Ahn, K. Li, S. Cai, Light or thermally powered autonomous rolling of an elastomer rod. *ACS Appl. Mater. Interfaces* **10**, 25689–25696 (2018).
65. L. Ren, Y. He, B. Wang, J. Xu, Q. Wu, Z. Wang, W. Li, L. Ren, X. Zhou, Q. Liu, B. Li, Z. Song, 4D printed self-sustained soft crawling machines fueled by constant thermal field. *Adv. Funct. Mater.* **34**, 2400161 (2024).
66. Y. Yu, C. Du, K. Li, S. Cai, Controllable and versatile self-motivated motion of a fiber on a hot surface. *Extreme Mech. Lett.* **57**, 101918 (2022).
67. A. Baumann, A. Sáchez-Ferrer, L. Jacomine, P. Martinoty, V. Le Houerou, F. Ziebert, I. M. Kulić, Motorizing fibres with geometric zero-energy modes. *Nat. Mater.* **17**, 523–527 (2018).
68. H. Arazoe, D. Miyajima, K. Akaike, F. Araoka, E. Sato, T. Hikima, M. Kawamoto, T. Aida, An autonomous actuator driven by fluctuations in ambient humidity. *Nat. Mater.* **15**, 1084–1089 (2016).
69. X. Chen, D. Goodnight, Z. Gao, A. H. Cavusoglu, N. Sabharwal, M. DeLay, A. Driks, O. Sahin, Scaling up nanoscale water-driven energy conversion into evaporation-driven engines and generators. *Nat. Commun.* **6**, 7346 (2015).
70. M. Choi, B. Shin, H.-Y. Kim, Hygromachines: Humidity-powered wheels, seesaws, and vehicles. *Soft Robot.* **10**, 1171–1180 (2023).
71. B. Shin, J. Ha, M. Lee, K. Park, G. H. Park, T. H. Choi, K.-J. Cho, H.-Y. Kim, Hygrobot: A self-locomotive ratcheted actuator powered by environmental humidity. *Sci. Robot.* **3**, eaar2629 (2018).
72. M. Hua, C. Kim, Y. Du, D. Wu, R. Bai, X. He, Swaying gel: Chemo-mechanical self-oscillation based on dynamic buckling. *Matter* **4**, 1029–1041 (2021).
73. A. Chakrabarti, G. P. T. Choi, L. Mahadevan, Self-excited motions of volatile drops on swellable sheets. *Phys. Rev. Lett.* **124**, 258002 (2020).
74. Y. Kim, J. van den Berg, A. J. Crosby, Autonomous snapping and jumping polymer gels. *Nat. Mater.* **20**, 1695–1701 (2021).
75. M. Yamada, M. Kondo, J. Mamiya, Y. Yu, M. Kinoshita, C. J. Barrett, T. Ikeda, Photomobile polymer materials: Towards light-driven plastic motors. *Angew. Chem. Int. Ed. Engl.* **47**, 4986–4988 (2008).
76. X. Qian, Y. Zhao, Y. Alsaid, X. Wang, M. Hua, T. Galy, H. Gopalakrishna, Y. Yang, J. Cui, N. Liu, M. Marszewski, L. Pilon, H. Jiang, X. He, Artificial phototropism for omnidirectional tracking and harvesting of light. *Nat. Nanotechnol.* **14**, 1048–1055 (2019).
77. H. Zhang, H. Zeng, A. Eklund, H. Guo, A. Priimagi, O. Ikkala, Feedback-controlled hydrogels with homeostatic oscillations and dissipative signal transduction. *Nat. Nanotechnol.* **17**, 1303–1310 (2022).
78. R. J. Field, M. R. Burger, *Oscillations and Traveling Waves in Chemical Systems* (Wiley, 1985).
79. S. Maeda, Y. Hara, R. Yoshida, S. Hashimoto, Peristaltic motion of polymer gels. *Angew. Chem. Int. Ed. Engl.* **47**, 6690–6693 (2008).
80. M. C. Huber, U. Jonas, S. M. Schiller, An autonomous chemically fueled artificial protein muscle. *Adv. Intell. Syst.* **4**, 2100189 (2022).
81. Y. Alapan, O. Yasa, B. Yigit, I. C. Yasa, P. Erkoc, M. Sitti, Microrobotics and microorganisms: Biohybrid autonomous cellular robots. *Annu. Rev. Control Robot. Auton. Syst.* **2**, 205–230 (2019).
82. L. Ricotti, B. Trimmer, A. W. Feinberg, R. Raman, K. K. Parker, R. Bashir, M. Sitti, S. Martel, P. Dario, A. Menciassi, Biohybrid actuators for robotics: A review of devices actuated by living cells. *Sci. Robot.* **2**, eaaq0495 (2017).
83. K. Y. Lee, S.-J. Park, D. G. Matthews, S. L. Kim, C. A. Marquez, J. F. Zimmerman, H. A. M. Ardoña, A. G. Kleber, G. V. Lauder, K. K. Parker, An autonomously swimming biohybrid fish designed with human cardiac biophysics. *Science* **375**, 639–647 (2022).
84. D. N. Beal, F. S. Hover, M. S. Triantafyllou, J. C. Liao, G. V. Lauder, Passive propulsion in vortex wakes. *J. Fluid Mech.* **549**, 385–402 (2006).
85. T. McGeer, Passive dynamic walking. *Int. J. Robot. Res.* **9**, 62–82 (1990).
86. R. Tedrake, T. W. Zhang, M. Fong, H. S. Seung, "Actuating a simple 3D passive dynamic walker," in *IEEE International Conference on Robotics and Automation, 2004. Proceedings. ICRA'04. 2004* (IEEE, 2004), vol. 5, pp. 4656–4661.
87. S. H. Collins, M. Wisse, A. Ruina, A three-dimensional passive-dynamic walking robot with two legs and knees. *Int. J. Robot. Res.* **20**, 607–615 (2001).

88. T. Jansen, *Theo Jansen: The Great Pretender* (Nai010 Publishers, 2016).
89. J. Rabault, R. A. Fauli, A. Carlson, Curving to fly: Synthetic adaptation unveils optimal flight performance of whirling fruits. *Phys. Rev. Lett.* **122**, 024501 (2019).
90. B. H. Kim, K. Li, J.-T. Kim, Y. Park, H. Jang, X. Wang, Z. Xie, S. M. Won, H.-J. Yoon, G. Lee, W. J. Jang, K. H. Lee, T. S. Chung, Y. H. Jung, S. Y. Heo, Y. Lee, J. Kim, T. Cai, Y. Kim, P. Prasopsukh, Y. Yu, X. Yu, R. Avila, H. Luan, H. Song, F. Zhu, Y. Zhao, L. Chen, S. H. Han, J. Kim, S. J. Oh, H. Lee, C. H. Lee, Y. Huang, L. P. Chamorro, Y. Zhang, J. A. Rogers, Three-dimensional electronic microfliers inspired by wind-dispersed seeds. *Nature* **597**, 503–510 (2021).
91. D. J. Preston, H. J. Jiang, V. Sanchez, P. Rothemund, J. Rawson, M. P. Nemitz, W.-K. Lee, Z. Suo, C. J. Walsh, G. M. Whitesides, A soft ring oscillator. *Sci. Robot.* **4**, eaaw5496 (2019).
92. P. Rothemund, A. Ainla, L. Belding, D. J. Preston, S. Kurihara, Z. Suo, G. M. Whitesides, A soft, bistable valve for autonomous control of soft actuators. *Sci. Robot.* **3**, eaar7986 (2018).
93. D. Drotman, S. Jadhav, D. Sharp, C. Chan, M. T. Tolley, Electronics-free pneumatic circuits for controlling soft-legged robots. *Sci. Robot.* **6**, eaay2627 (2021).
94. M. Wehner, R. L. Truby, D. J. Fitzgerald, B. Mosadegh, G. M. Whitesides, J. A. Lewis, R. J. Wood, An integrated design and fabrication strategy for entirely soft, autonomous robots. *Nature* **536**, 451–455 (2016).
95. Y. Zhai, J. Yan, A. De Boer, M. Faber, R. Gupta, M. T. Tolley, Monolithic desktop digital fabrication of autonomous walking robots. *Adv. Intell. Syst.* 10.1002/aisy.202400876 (2025).
96. X. Yang, L. Chang, N. O. Pérez-Arancibia, An 88-milligram insect-scale autonomous crawling robot driven by a catalytic artificial muscle. *Sci. Robot.* **5**, eaba0015 (2020).
97. H. Zeng, O. M. Wani, P. Wasylczyk, A. Priimagi, Light-driven, caterpillar-inspired miniature inching robot. *Macromol. Rapid Commun.* **39**, 1700224 (2018).
98. A. W. Feinberg, A. Feigel, S. S. Shevkoplyas, S. Sheehy, G. M. Whitesides, K. K. Parker, Muscular thin films for building actuators and powering devices. *Science* **317**, 1366–1370 (2007).
99. S. Maeda, Y. Hara, T. Sakai, R. Yoshida, S. Hashimoto, Self-walking gel. *Adv. Mater.* **19**, 3480–3484 (2007).
100. Z. Deng, K. Li, A. Priimagi, H. Zeng, Light-steerable locomotion using zero-elastic-energy modes. *Nat. Mater.* **23**, 1728–1735 (2024).
101. Y. Zhao, Y. Hong, F. Qi, Y. Chi, H. Su, J. Yin, Self-sustained snapping drives autonomous dancing and motion in free-standing wavy rings. *Adv. Mater.* **35**, e2207372 (2023).
102. F. Qi, Y. Li, Y. Hong, Y. Zhao, H. Qing, J. Yin, Defected twisted ring topology for autonomous periodic flip-spin-orbit soft robot. *Proc. Natl. Acad. Sci. U.S.A.* **121**, e2312680121 (2024).
103. A. Kotikian, C. McMahan, E. C. Davidson, J. M. Muhammad, R. D. Weeks, C. Daraio, J. A. Lewis, Untethered soft robotic matter with passive control of shape morphing and propulsion. *Sci. Robot.* **4**, eaax7044 (2019).
104. Y. Zhao, Y. Chi, Y. Hong, Y. Li, S. Yang, J. Yin, Twisting for soft intelligent autonomous robot in unstructured environments. *Proc. Natl. Acad. Sci. U.S.A.* **119**, e2200265119 (2022).
105. X. Zhou, G. Chen, B. Jin, H. Feng, Z. Chen, M. Fang, B. Yang, R. Xiao, T. Xie, N. Zheng, Multimodal autonomous locomotion of liquid crystal elastomer soft robot. *Adv. Sci.* **11**, 2402358 (2024).
106. A. J. Smits, Undulatory and oscillatory swimming. *J. Fluid Mech.* **874**, P1 (2019).
107. T. Zhao, Y. Fan, J. Lv, Photomorphogenesis of diverse autonomous traveling waves in a monolithic soft artificial muscle. *ACS Appl. Mater. Interfaces* **14**, 23839–23849 (2022).
108. A. Maghsoodi, K. Bhattacharya, Light-induced swirling and locomotion. *Proc. R. Soc. A Math. Phys. Eng. Sci.* **478**, 20220545 (2022).
109. Z. Deng, H. Zhang, A. Priimagi, H. Zeng, Light-fueled nonreciprocal self-oscillators for fluidic transportation and coupling. *Adv. Mater.* **36**, 2209683 (2024).
110. G. Vantomme, L. C. M. Elands, A. H. Gelebart, E. W. Meijer, A. Y. Pogromsky, H. Nijmeijer, D. J. Broer, Coupled liquid crystalline oscillators in Huygens' synchrony. *Nat. Mater.* **20**, 1702–1706 (2021).
111. Z. Li, N. V. Myung, Y. Yin, Light-powered soft steam engines for self-adaptive oscillation and biomimetic swimming. *Sci. Robot.* **6**, eabi4523 (2021).
112. J. Gau, J. Lynch, B. Aiello, E. Wold, N. Gravish, S. Sponberg, Bridging two insect flight modes in evolution, physiology and robophysics. *Nature* **622**, 767–774 (2023).
113. G. Vantomme, A. H. Gelebart, D. J. Broer, E. W. Meijer, A four-blade light-driven plastic mill based on hydrazone liquid-crystal networks. *Tetrahedron* **73**, 4963–4967 (2017).
114. D. Wang, Z. Chen, M. Li, Z. Hou, C. Zhan, Q. Zheng, D. Wang, X. Wang, M. Cheng, W. Hu, B. Dong, F. Shi, M. Sitti, Bioinspired rotary flight of light-driven composite films. *Nat. Commun.* **14**, 5070 (2023).
115. Q. Cheng, W. Cheng, Y. Dai, K. Li, Self-oscillating floating of a spherical liquid crystal elastomer balloon under steady illumination. *Int. J. Mech. Sci.* **241**, 107985 (2023).
116. D. Ge, K. Li, Pulsating self-snapping of a liquid crystal elastomer bilayer spherical shell under steady illumination. *Int. J. Mech. Sci.* **233**, 107646 (2022).
117. W. Hu, G. Z. Lum, M. Mastrangeli, M. Sitti, Small-scale soft-bodied robot with multimodal locomotion. *Nature* **554**, 81–85 (2018).
118. F. Ling, H. Guo, E. Kanso, Instability-driven oscillations of elastic microfilaments. *J. R. Soc. Interface* **15**, 20180594 (2018).
119. Y. Yao, A. M. Wilborn, B. Lemaire, F. Trigka, F. Stricker, A. H. Weible, S. Li, R. K. A. Bennett, T. C. Cheung, A. Grinthal, M. Zhernekov, G. Freychet, P. Wąsik, B. Kozinsky, M. M. Lerch, X. Wang, J. Aizenberg, Programming liquid crystal elastomers for multistep ambidirectional deformability. *Science* **386**, 1161–1168 (2024).
120. B. Zuo, M. Wang, B.-P. Lin, H. Yang, Visible and infrared three-wavelength modulated multi-directional actuators. *Nat. Commun.* **10**, 4539 (2019).
121. Q. He, R. Yin, Y. Hua, W. Jiao, C. Mo, H. Shu, J. R. Raney, A modular strategy for distributed, embodied control of electronics-free soft robots. *Sci. Adv.* **9**, eade9247 (2023).
122. H. Zhang, H. Zeng, A. Priimagi, O. Ikkala, Viewpoint: Pavlovian materials—Functional biomimetics inspired by classical conditioning. *Adv. Mater.* **32**, e1906619 (2020).
123. K. Li, B. Zhang, Q. Cheng, Y. Dai, Y. Yu, Light-fueled synchronization of two coupled liquid crystal elastomer self-oscillators. *Polymers* **15**, 2886 (2023).
124. K. Tunstrøm, Y. Katz, C. C. Ioannou, C. Huepe, M. J. Lutz, I. D. Couzin, Collective states, multistability and transitional behavior in schooling fish. *PLoS Comput. Biol.* **9**, e1002915 (2013).
125. T. Po, E. Kanso, M. J. McHenry, Cooperative transport in sea star locomotion. *Curr. Biol.* **34**, 2551–2557.e4 (2024).
126. S. Li, M. M. Lerch, J. T. Waters, B. Deng, R. S. Martens, Y. Yao, D. Y. Kim, K. Bertoldi, A. Grinthal, A. C. Balazs, J. Aizenberg, Self-regulated non-reciprocal motions in single-material microstructures. *Nature* **605**, 76–83 (2022).
127. M. Zhang, A. Pal, X. Lyu, Y. Wu, M. Sitti, Artificial-goosebump-driven microactuation. *Nat. Mater.* **23**, 560–569 (2024).
128. T. Chen, M. Pauly, P. M. Reis, A reprogrammable mechanical metamaterial with stable memory. *Nature* **589**, 386–390 (2021).
129. J. Byun, A. Pal, J. Ko, M. Sitti, Integrated mechanical computing for autonomous soft machines. *Nat. Commun.* **15**, 2933 (2024).
130. Y. Jiang, L. M. Korpas, J. R. Raney, Bifurcation-based embodied logic and autonomous actuation. *Nat. Commun.* **10**, 128 (2019).
131. G. Stano, G. Percoco, Additive manufacturing aimed to soft robots fabrication: A review. *Extreme Mech. Lett.* **42**, 101079 (2021).
132. S. Zhang, X. Ke, Q. Jiang, Z. Chai, Z. Wu, H. Ding, Fabrication and functionality integration technologies for small-scale soft robots. *Adv. Mater.* **34**, e2200671 (2022).

Acknowledgments: We thank H. Liu and Y. Chen at Shanghai Jiao Tong University for support. **Funding:** This work was supported by the Air Force Office of Scientific Research award FA955017-1-0311 and the Office of Naval Research awards N000141712117 and N000142212595. **Author contributions:** Conceptualization: C.C., P.S., and X.H. Funding acquisition: X.H. Supervision: C.C. and X.H. Writing—original draft: C.C., P.S., Z.L., S.D., M.S., C.Z., Y.D., Y.Y., T.J.W., R.K.-B., M.S., T.I., and X.H. Writing—review and editing: C.C., P.S., Z.L., M.S., T.I., and X.H. **Competing interests:** The authors declare that they have no competing interests.

Submitted 30 July 2024
Accepted 30 April 2025
Published 28 May 2025
10.1126/scirobotics.ads1292